

# Earth ArXiv

**Title:** A generalized additive mixed-effect modeling approach for characterizing Sentinel-2 surface reflectances of visible light from Torch Lake in Antrim County, Michigan, 2019-2025

**Author:** David J. Holtschlag, Hydrologist

**Affiliation:** Retired

**Email:** dholtschlag@outlook.com

**This is a non-peer-reviewed preprint submitted to EarthArXiv.**

A generalized additive mixed-effect modeling approach for  
characterizing Sentinel-2 surface reflectances of visible light from  
Torch Lake in Antrim County, Michigan, 2019-2025

David J. Holtschlag

November 26, 2025

# Contents

Abbreviations . . . . .	5
Abstract . . . . .	7
Introduction . . . . .	7
Purpose and Scope . . . . .	7
Study Area Description . . . . .	8
Previous and On-Going Data Collection and Analysis Studies . . . . .	8
Flow through Torch Lake . . . . .	11
Data Used in the Report . . . . .	12
Sentinel 2 Satellite Imagery . . . . .	12
Bathymetry Data . . . . .	13
AI-Assisted Analysis Workflow . . . . .	14
Data Features and Preparation . . . . .	14
Satellite Overpass . . . . .	14
Horizontal Masking and Stratification of Torch Lake . . . . .	17
Statistical Distribution of Reflectances . . . . .	19
Time Series of Reflectance Data . . . . .	19
Statistical Modeling Approach . . . . .	23
Modeling Framework . . . . .	23
Modeling Equation . . . . .	23
Model Specifications . . . . .	24
Model Selection Criteria . . . . .	25
Model Selection . . . . .	26
Discussion . . . . .	28
Fixed Effects Associated with Water-Depth Intervals, Satellite Orbit, and Trend . . . . .	28
Smooth Effects Describing Seasonal Variations by Depth and Cloud Score Associations . . . . .	30
Random Effects and Error Correlation . . . . .	36
GAMM ID3: Spatial Random Intercepts and Temporal Error Correlation . . . . .	36
GAMM ID4: Temporal Random Intercepts and Spatial Error Correlation . . . . .	39
Conclusions . . . . .	42
References Cited . . . . .	43
Appendices . . . . .	44
Appendix 1. Acknowledgements . . . . .	44

---

Appendix 2. Horizontal strata partitioning of Torch Lake with GAMM ID3 spatial random intercepts. . . . .	45
Appendix 3. JavaScript used in Google Earth Engine to access imagery by An- thropic's Claude, September 2025 . . . . .	47

## Figures

1	Vicinity map of Torch Lake in Antrim County, Michigan . . . . .	10
2	Streamgages monitoring flows into and out from Torch Lake in Antrim County, MI .	12
3	Solar azimuth and zenith angle of Sentinel-2 images for Torch Lake in Antrim County, Michigan . . . . .	15
4	Differences between reflectances of blue, green, and red light from Torch Lake obtained by Sentinel 2A and 2B satellites on April 11, 2025 by color band and water-depth interval . . . . .	16
5	Torch Lake with 60 subbasins and the central points of each subbasin polygon in Antrim County, Michigan . . . . .	18
6	Median surface reflectances of Sentinel 2 data from Torch Lake by water-depth interval and color band . . . . .	20
7	Time-series plots of blue, green, and red surface reflectances from all northern strata in Torch Lake, Antrim County, Michigan . . . . .	21
8	Time-series plots of blue, green, and red surface reflectances from all southern strata in Torch Lake, Antrim County, Michigan . . . . .	22
9	Variation of reflectance intensity with cloud score . . . . .	31
10	Seasonal variation of Sentinel 2 reflectances by color band and depth intervals from Torch Lake in Antrim County, Michigan . . . . .	32
11	Seasonal variation of Landsat reflectances by color band and depth intervals from Torch Lake in Antrim County, Michigan . . . . .	33
12	Composite satellite images of Torch Lake showing seasonal reflectances for the weeks of April 10 and July 9 during 2019-2025 in Antrim County, Michigan . . . . .	34
13	Composite satellite images of Torch Lake showing seasonal reflectances for the weeks of September 7 and December 1 during 2019-2025 in Antrim County, Michigan . . . . .	35
14	Torch Lake with strata fill colors based on GAMM ID3 spatial random intercepts in Antrim County, Michigan . . . . .	38
15	Relation between error correlation and temporal separation distances between selected images on Torch Lake in Antrim County, Michigan . . . . .	39
16	Random temporal intercepts by date of Sentinel 2 image of Torch Lake in Antrim County, Michigan . . . . .	40
17	Spatial correlation of GAMM ID4 errors as a function of strata separation distances	41

## Tables

2	Comparison of GAMM ID4 BIC fit statistics for alternative spatial correlation functions	27
3	Comparison of alternative GAMM forms to estimate surface reflectance from Torch Lake in Antrim County, Michigan . . . . .	27
4	Fixed effect terms for band reflectances from Torch Lake in Antrim County, Michigan	29
5	Smooth terms from GAMM for Sentinel 2 band reflectances from Torch Lake in Antrim County, Michigan . . . . .	30
1	Strata naming, water-depths, area, and locational information for Torch Lake in Antrim County, Michigan . . . . .	45

## Abbreviations

Identifier	Definition
Cloud Score+	A quality assessment (QA) processor to identify relatively clear pixels and effectively remove clouds and cloud shadows from surface reflectance data.
Digital Number (DN)	Digital numbers are integers representing fractional reflectances values multiplied by 10000 and then rounded to zero digits.
Depth	A factor variable that describes water-depth intervals ‘5-50’, ‘50-100’, ‘100-200’, or ‘200-300’ feet with a reference interval of ‘0-5’ feet.
edf	Effective degrees of freedom is a statistic for a smooth component of a GAM. The higher the edf, the greater flexibility of the corresponding smoothing spline and the greater the chance of over fitting.
ESA	European Space Agency
EST	Eastern Standard Time (UTC minus 5 hours)
GAM	A Generalized Additive Model is a type of regression model that contains both parametric and smooth terms. GAMs are used to attribute variations in $\vec{R}$ or $\vec{R}$ to variations in factor variables, like satellite (SAT) number (Landsat 5, 7, 8, or 9), or smooth variations in seasonal or local levels.
GBA	Golden Brown Algae, Chrysophytes chrysomonads, are a group of non-toxic aquatic organisms that are common in oligotrophic lakes, which consist primarily of diatoms along with blue-green and green algae, bacteria, and fungi.
GEE	Google Earth Engine, a catalog of satellite imagery and geospatial datasets with planetary-scale capabilities.
GIS	A Geographic Information System is a computer system that can be used to analyze and display geographically referenced information.
Intercept	An estimated parameter in a GAM that describes the mean reflectance given the variations in the explanatory variables.
MI GeoRef	An Oblique Mercator map projection with special parameters for Michigan based on the North American Datum of 1983
N	The number of measurements or observation used in model development.
NASA	National Aeronautics and Space Administration
NHDPlus HR	A geospatial dataset depicting the flow of water through the stream network in the United States. NHDPlus HR was built on a 1:24,000 scale or more detailed data set and the 10-meter 3D USGS Elevation Program data.
NOAA	National Oceanic and Atmospheric Administration
Orbit	Sentinel 2 satellites require 143 orbits to obtain a complete image of the earth. Images from relative orbits identified as R083 and R126, located to the right and left of Torch Lake, respectively, were obtained during the north to south transit of the orbit.
p-value	A statistic to describe the probability of obtaining the observed results from available data given that the null hypothesis is true. For example, the null hypothesis commonly assumes that a variable in a statistical model is insignificant. The smaller the p-value, the less likely it is that the null hypothesis is true. If the null hypothesis is rejected, the variable is maintained in the statistical model.

Identifier	Definition
Pixel	A pixel (picture element) is the smallest unit in a digital satellite image. Each pixel represents the average intensity of the band width interval it represents. No reflectance corresponds to a value of zero and reflectance of all light received equals 1. Pixels elements representing different optical bands, such as red, green, and blue, can be composited to represent natural colors.
$\mathcal{R}$	Sentinel 2 measured surface reflectance values that generally occurring with the range of 0 to 1.
$\dot{\mathcal{R}}$	$\dot{\mathcal{R}}$ values that are trimmed to the interval from $[0, 0.2]$ , where most measured reflectance values fall within.
$\ddot{\mathcal{R}}$	$\dot{\mathcal{R}}$ values that are square-root transformed to help normalize their distributions for all bands.
Ref.df	Reference degrees of freedom is a property of the smooth component in a GAM. The Ref.df reflects the maximum degrees of freedom possible for the form of the smooth specified.
Reflectance	Pixel reflectance refers to the fraction of incoming solar radiation that is reflected back into space. This fraction is generally constrained to the interval from 0 to 1. In a deep lake, liquid water commonly has a reflectance from 0-0.2, while snow may have a reflectance near 1.
ROI	Region of Interest delineate specific areas or subareas of lake surfaces.
Sentinel-2A	ESA satellite with sun-synchronous near-polar orbit launched on June 23, 2015, having a 10-day repeat imaging cycle.
Sentinel-2B	ESA satellite launched on March 7, 2017, also having 10-day repeat imaging cycle but staggered in time to provide a 5-day repeat imaging cycle when combined with Sentinel-2A data.
SR	Surface Reflectance is a property of the reflector that can be expressed as the ratio of the amount of light reflected by a surface to the amount of light striking the surface. Surface Reflectance is commonly subdivided into the wavelength intervals (narrow bands) of light.
TLPA	Torch Lake Protection Alliance
TSI	Tropic Status Index is a method to describe the biological productivity of a lake.
USGS	U.S. Geological Survey
UTC	Coordinated Universal Time

# A generalized additive mixed-effect modeling approach for characterizing Sentinel-2 surface reflectances of visible light from Torch Lake in Antrim County, Michigan, 2019-2025

by David J. Holtschlag, Hydrologist

## Abstract

A generalized additive model (GAM) and three generalized additive mixed-effect models (GAMMs) were developed and compared to describe variations of surface reflectances of visible light from Torch Lake in the blue, green, and red bands from Sentinel 2 satellite imagery. All models included fixed effects associated with water-depth intervals, satellite orbits, trend, and smooth effects associated with season by water depth, and a measure of cloudiness. The GAMM models also included random effects of strata or timing, and spatial or temporal correlation effects. The analysis was based on 287 European Space Agency's Sentinel 2A, 2B, and 2C satellite images of Torch Lake in Antrim County, Michigan, obtained from 2019 to 2025. The approach is motivated by the recognition of multiple sources of randomness that affect model uncertainty, where, at least one of which, is separable. Primary sources of randomness include day-to-day variations in surface reflectances from the water surface and sensor measurement uncertainties. A separable source of randomness is the uncorrected atmospheric distortions through which light passes from the sun to the lake surface and back to the satellite sensors. Results indicated that the GAMM models with random effects were more accurate than the GAM model without them. The preferred GAMM model accounted for error correlation of median reflectances in 60 strata spanning the surface of Torch Lake and a random temporal intercept component associated with the uncertainties in corrections for daily atmospheric conditions. Seasonal changes in reflectances within the 0-5 ft water-depth interval had lower magnitudes and were out of phase with seasonal variability in the three deeper water-depth intervals. Changes in reflectances in shallow areas may be more indicative of changes in reflectance within benthic areas, whereas changes in deeper areas may be related to dissolved and suspended materials in the water column. The uncertainty of shallow-water depths degrades the interpretability of surface reflections from strata in shallow waters.

## Introduction

Introductory material includes background information on the circumstances and motivations for the study, purpose and scope, a description of the study area, the attributes and limitations of available data, and the role of an AI-assistant in developing the report.

## Purpose and Scope

The purpose of this report is to characterize the spatial and temporal components of surface-reflectances from Torch Lake using continual Sentinel 2 images, and to help provide a basis for understanding the dynamic, interrelated physical, chemical, and biological processes occurring within the lake. Point information on these processes are provided at discrete times and

locations by field water-quality measurements. Information on surface reflectances are intended to guide discrete water-quality sampling times and locations, and to extend the utility of discrete field measurements to the time span of continual satellite measurements. Integration of continual and discrete measurements is intended to help inform water-quality management decisions for Torch Lake.

## Study Area Description

Torch Lake is in Antrim County, Michigan, and is part of a Chain of Lakes that extends about 55 miles from Beals Lake in eastern Antrim County downstream to the East Arm of Grand Traverse Bay (fig. 1). Torch Lake has a surface area of  $29.3 \text{ mi}^2$ , and a maximum depth of about 300 ft. The scenic lake is highly oligotrophic, but there is concern about the recent proliferation of golden-brown algae (Chrysophyta, Chrysophyceae) in the benthic zone.

The boundaries of Torch Lake are based on the USGS National Hydrography Dataset Plus High Resolution (NHDPlus HR) geospatial dataset (U.S. Geological Survey 2020). The drainage area of Torch Lake Basin monitored at the outlet on Torch River is  $275.3 \text{ mi}^2$ . The inset map (fig. 1) highlights the location of Antrim County in Michigan and two orbital paths of Sentinel 2 satellites (in yellow) that provided images for this analysis.

## Previous and On-Going Data Collection and Analysis Studies

USGS obtained discrete water-quality samples from Torch Lake in the north and south basins (U.S. Geological Survey (2003a), and U.S. Geological Survey (2003b)). The data includes from 21 to 34 samples of major inorganics and non-metals, along with physical measurements of specific conductance, water temperature, and pH.

Stevenson (2016) analyzed the relation between the presence, abundance, and algal species composition of golden-brown algae (GBA) in Torch Lake, Lake Bellaire, and Clam Lake. GBA is a benthic algae composed primarily of diatoms with lesser amounts of cyanobacteria and green algae, that attaches to or lives-in sand or attaches to rocks on the bottom of lakes. As a photo-synthesizer, however, GBA can only thrive in the photic zone, which is limited by depth and water-clarity. In contrast to benthic algae, plankton algae (phytoplankton), are photosynthesizing plants suspended in the near-surface water column.

The Torch Lake Protection Alliance (TLPA) coordinates with volunteers from Tip of the Mitt Watershed Council (2024) and Three Lakes Association (2004), who have provided additional monitoring and reporting of water quality in the north and south basins of the Torch Lake from 2014 to 2021. The water-quality monitoring team has characterized the presence of GBA by a visual “scuzziness score,” a metric which ranges from 0 to 10, with 10 being the highest amount and darkest color of GBA. Stevenson shows that diatom species composition and abundance varied among lakes and by season, but found little relation between scuzziness scores and phosphorus or nitrogen levels.

In cooperation with Antrim County, Michigan, the USGS initiated a comprehensive water-quality study of Torch Lake in 2023 led by Drs. Dale M. Robertson and Sherry Martin, which is on-going. The study plan includes extensive field-data collection and analysis to better understand the flow system, nutrient dynamics, and biological characteristics of the lake.

Holtschlag (2024) characterized seasonal and long-term variations in surface reflectances within the blue, green, and red bands of visible light from Torch Lake using Landsat images obtained

from 1984 to 2023. This analysis included five water-depth factors and two (north and south) basin factors, which together formed 10 strata. Thus, the surface reflectances of each satellite image included in the analysis was characterized by 10 median reflectances within each strata. Randomly varying atmospheric conditions between satellite images, however, likely affected reflectance measurements from all strata in a similar way, so the possibility of correlation among model errors was informally explored. Although likely error correlations were characterized, the magnitude of these correlations were considered insufficient to substantially degrade the high significance of the model terms, which generally had p-values  $\ll 0.0001$ , with models that explained about 74.0, 81.5, and 63.8 percent of the variability of blue, green, and red bands of visible light, respectively.

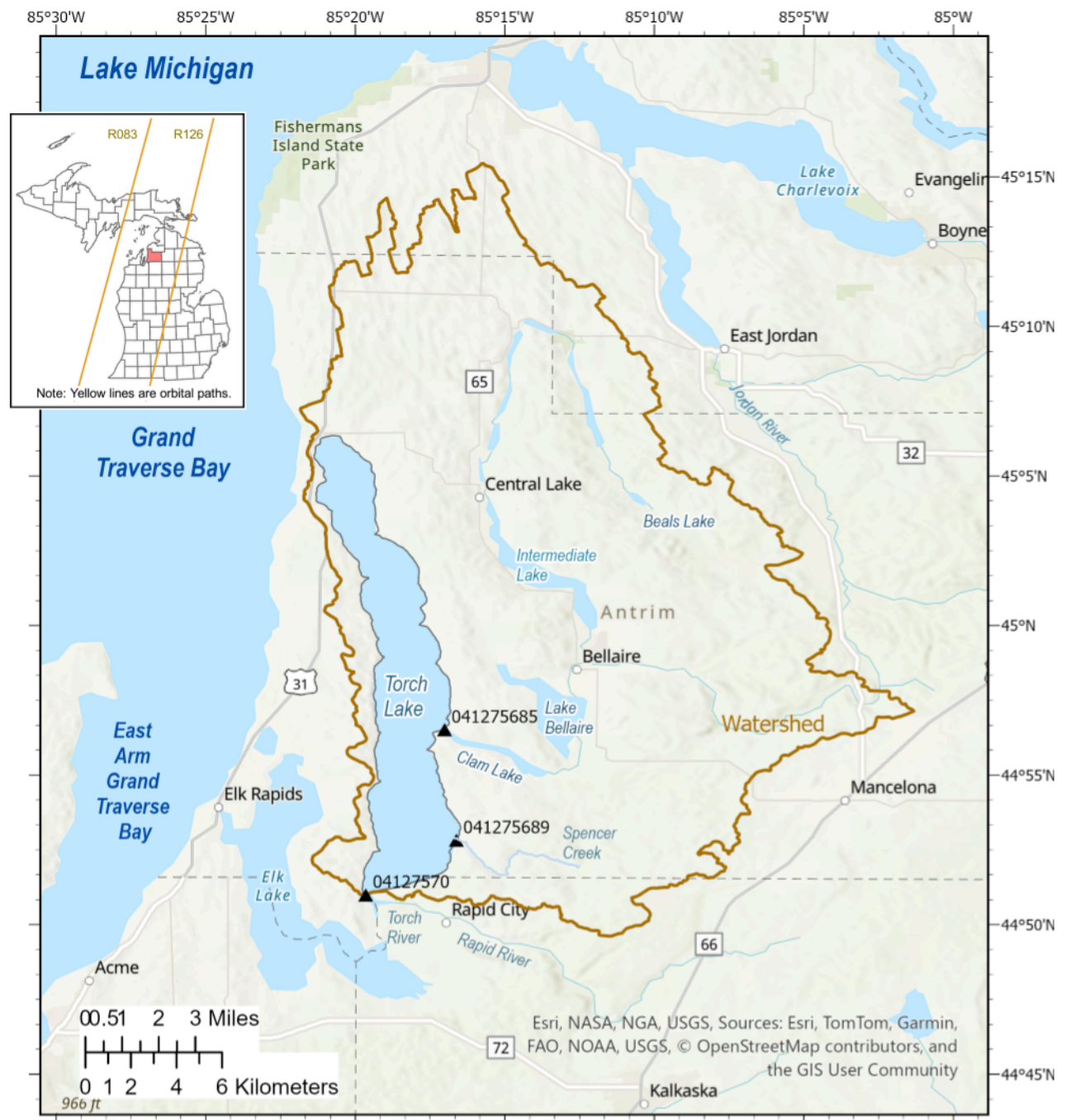


Figure 1. Vicinity map of Torch Lake in Antrim County, Michigan

## Flow through Torch Lake

Tributary flows are monitored at three locations near Torch Lake (fig. 2). Inflows are measured at USGS streamgage 041275685 Clam Lake Outlet to Torch Lake near Alden, MI, and at 041275689 Spencer Creek at (near 10520) Coy Street in Alden, MI. Outflow is monitored at 04127570 Torch River at County Road 593 at Torch River, MI. Together, the drainage areas of the monitored inflows accounts for about 76 percent of the drainage areas monitored at the outflow. Nearly half of the unmonitored drainage area consists of the surface area of Torch Lake itself.

The primary inflow to Torch Lake is monitored at the Clam Lake Outlet streamgage, which is located about 120 ft upstream from Torch Lake near River Street along a 0.22 mi connecting channel between the outlet of Clam Lake and Torch Lake. The streamgage is at north latitude  $44^{\circ}56'33.01''$  and west longitude  $85^{\circ}17'0.96''$ . The drainage area at streamgage 041275685 is  $198.8 \text{ mi}^2$ . Streamgage records available from April 18, 2023 to April 18, 2025 indicate an average flow of  $333 \text{ ft}^3/\text{s}$ , and an average water level of 589.6 ft, based on a gage datum of 574.28 ft (NAVD88).

Inflow is also monitored at USGS streamgage 041275689 Spencer Creek at Coy Street in Alden, MI, about 400 ft upstream from the mouth of Spencer Creek on Torch Lake. The streamgage is at north latitude  $44^{\circ}52'51.19''$  and west longitude  $85^{\circ}16'37.25''$ . The drainage area at streamgage is  $10.48 \text{ mi}^2$ . Flow records from April 18, 2023, to April 18, 2025, indicate an average flow of  $5.61 \text{ ft}^3/\text{s}$ .

Outflow from Torch Lake is monitored at 04127570 Torch River at County Road 593 at Torch River, MI, which is about 120 ft upstream from the outlet of Torch Lake to Torch River. The streamgage is located at north latitude  $44^{\circ}51'1.44''$  and west longitude  $85^{\circ}19'39.98''$ . The drainage area at this gage is  $275.3 \text{ mi}^2$ . Flow records from April 18, 2023 to April 18, 2025, indicate the average flow was  $398 \text{ ft}^3/\text{s}$ .

Flows at all streamgages are computed based on of an index velocity rating (Levesque and Oberg 2012). The difference between the inflows flows from Clam Lake Outlet and Spencer Creek to Torch River are attributed to flow from unmonitored parts of the basin, differences between direct precipitation and evaporation from the surface of Torch Lake, and possible changes in the volume of water stored in Torch lakes within the period.

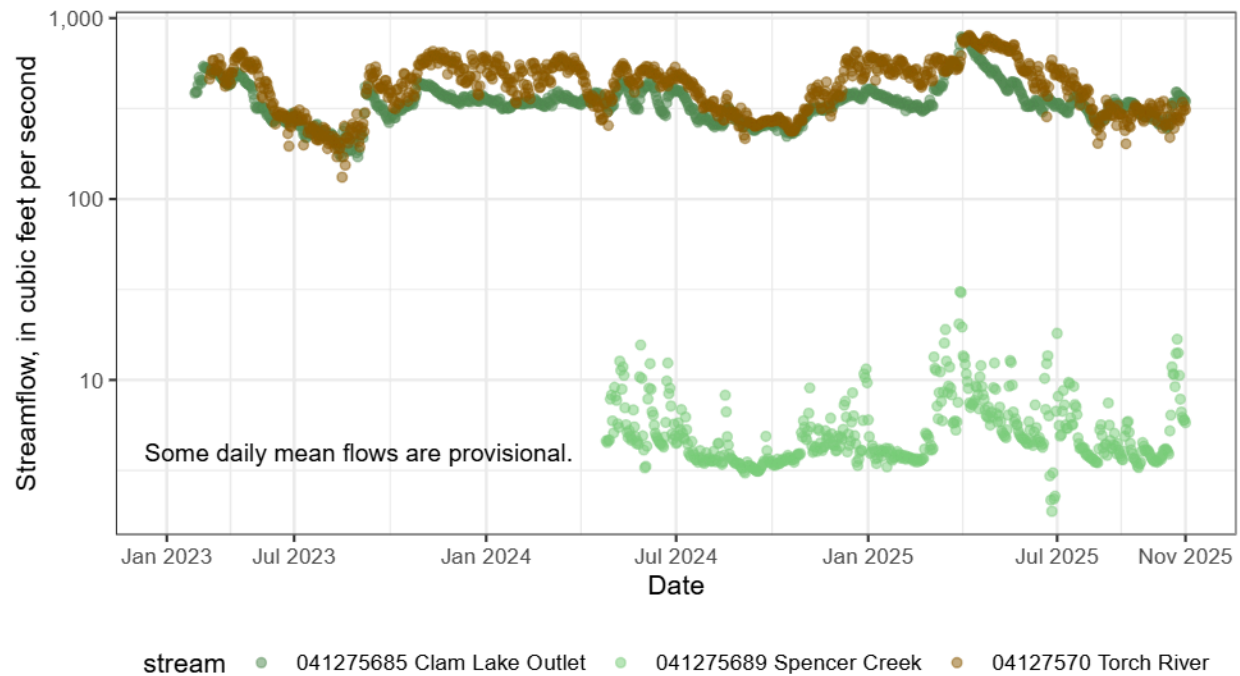


Figure 2. Streamgages monitoring flows into and out from Torch Lake in Antrim County, MI

## Data Used in the Report

The primary data used in this report is the Sentinel 2 satellite imagery and bathymetry data for Torch Lake. All data are from publicly available sources. The javascript used to retrieve statistics of Sentinel 2 imagery within the Google Earth Engine environment are included as an appendix in the report to facilitate the reproducibility.

## Sentinel 2 Satellite Imagery

Imagery for this analysis were from the ESA Copernicus Sentinel-2 mission, which at the time of this study, included three satellites (Sentinel-2A/2B/2C) (European Space Agency 2025). Sentinel satellites 2A, 2B, and 2C were launched in 2015, 2017, and 2024, respectively. Each satellite is expected to be operational for about a decade. Sentinel 2A is being replaced by 2C, and 2B will eventually be replaced by 2D.

Sentinel-2 satellites have a near polar, sun-synchronous orbit at an altitude of 786 km. Both satellites have a 10-day repeat cycle, but are phased 180 degrees apart, which results in an effective 5-day repeat cycle at the equator. Due to a constant image swath width of 290 km and the convergence of orbital paths with increasing distance from the equator, more frequent repeats are possible. In particular, images from relative orbits R083 and R126 (shown as golden diagonal lines on fig. 1 inset) both span Torch Lake, which has a center near 45-degrees north latitude, and provides opportunities for images as short as 2- and 3-days apart. Many more days between repeat images were common, however, because of clouds, atmospheric conditions, and ice. Figure 3A shows histograms of the frequency of images with time of day by satellite and orbit. Note that solar azimuth (fig. 3B) is more sensitive to orbit than is solar zenith (fig. 3C).

Sentinel-2 satellites carry a Multispectral Imager (MSI) covering 13 spectral bands (443–2190 nm). The spatial resolutions are defined by a single pixel (picture element) in the satellite image that represents a square 10 m on a side (four visible and near-infrared bands), 20 m on a side (six red-edge/shortwave-infrared bands) and 60 m on a side (three atmospheric correction bands). Surface reflectance data from visible light in the blue band (458–523 nm), green band (543–578 nm), and red band (650–680 nm) were used to characterize reflectances.

Raw surface reflectance values  $\mathcal{R}$  in the range from [0,1] are multiplied by 10000 and then stored and transmitted as 15-bit unsigned integer values referred to as digital numbers (DN). When harmonized, the DN are used for efficient storage and transmission of reflectance values. Surface reflectances  $\hat{\mathcal{R}}$  are rescaled DN values  $\min(0, (\text{DN} / 10000))$ .

Sentinel-2 Cloud Score values (CloudScore+) were used as a quality assessment tool. CloudScore+ is a continuous value between 0 and 1 that represents the likelihood of a pixel being clear, with 0 representing not clear (occluded) and 1 representing clear. In this analysis, the CloudScore+ was taken as a measure of the average score in each stratum.

All Sentinel-2 images group 10m x 10m pixels into square tiles representing 109.8 km on a side, with an overlap of 4,900 m between adjacent tiles. In this analysis, all images were identified as tile 16TFQ, based loosely on the Military Grid Reference System (MGRS). In tile IDs, the first 2-digits indicate the UTM (Universal Transverse Mercator) zone and the first character (T) represents the latitude zone of the image containing Torch Lake.

Sentinel-2 data for the period January 6, 2019, to September 16, 2025, represented the period of usable data at the beginning of the study. Individual images were visually screened to assess the likely utility of images for this analysis. Cloudiness extent, haze conditions, and surface ice commonly degraded reflectance data to varying degrees among these images. Of the images available, 287 were selected to represent Torch Lake reflectances during the period. All selected images were processed to level L2A, which provides orthorectified surface reflectance data also known as Bottom Of the Atmosphere (BOA) or surface reflectance data in contrast to Top of the Atmosphere (TOA) data. It also includes Scene Classification, Aerosol Optical Thickness, and Water Vapor data.

### Bathymetry Data

Bathymetry data for Torch Lake was obtained from the Michigan's Open GIS Data Repository for Inland Lake Contours (Michigan Department of Natural Resources 2023). These data were used to define five water-depth intervals of: 0–5 ft, 5–50 ft, 50–100 ft, 100–200 ft, and 200–300 ft. The 250-ft depth contour available in the bathymetry was omitted because the surface reflectances were not thought to differ substantially from the reflectance between 200 and 250 ft and 250 and 300 ft. Contours of bathymetry data are necessary, but are limited to fairly wide discrete intervals. Light absorption in the water column is highly sensitive to water depth so the analysis is limited by the coarseness of the bathymetry data especially at shallower (<50 ft) depths.

Future studies may benefit from the availability of recent (since 2019) ICESat-2 data that provides detailed along-track shallow-water bathymetry based on the satellite's photon-counting laser altimeter (Jasinski, M. F., J. D. Stoll, D. Hancock, and the ICESat-2 Science Team 2023). Preliminary assessment discovered numerous track across Torch Lake with photons returning from a maximum depth of about 50 ft. This instrument may provide a basis for developing a digital elevation model (DEM) of shallow water bathymetry at a scale comparable to the spatial

resolution of Sentinel 2 (10 m) or Landsat (30 m) data. This type of information would help in the development of continuous model of depth-effects on shallow-water reflectances

### AI-Assisted Analysis Workflow

This analysis was conducted in partnership with Claude (Anthropic), a large language model AI assistant, which facilitated multiple aspects of the remote sensing data processing and statistical analysis workflow. The AI collaboration included:

- \* Code development: JavaScript for Google Earth Engine data access and R code for statistical modeling, with iterative debugging and optimization
- \* Methodological consultation: Discussion of appropriate GAMM structures for spatiotemporal correlation
- \* Document preparation: LaTeX formatting, figure generation code, and manuscript structure
- \* Literature integration: Synthesis of relevant remote sensing and statistical modeling approaches

This collaborative approach exemplifies how AI tools can augment scientific workflows in remote sensing applications, particularly for complex spatiotemporal analyses requiring integration of multiple software environments. The human author is responsible for all errors in the report that arose from any source.

## Data Features and Preparation

This section discusses satellite overpass timing for different orbital paths, and comparison of satellite images 2A and 2B, which occurred during a transition on April 11, 2025. In addition, horizontal stratification of Torch Lake is described and the strata codes are described.

### Satellite Overpass

Figure 3 A shows the timing of Sentinel 2A, 2B, and 2C overpasses by orbital path. Generally, the images from orbital path R083 occurred at about 11:28 AM, and images from orbital path R126 were obtained about 11 minutes later at 11:39 AM (Eastern Standard Time).

Figure 3 B shows mean solar azimuth angles (horizontal angles measured clockwise from 0-degrees north) greater than 150 degrees (south southeast) on July 1 of the year, and minimum azimuths of about 168 degrees in mid-November. Azimuth values for orbital path R083 were consistently greater than azimuths for orbital path R126, with a maximum difference of about 5 degrees. Figure 3 C shows greater consistency between mean solar zenith angles (vertical angles from zenith down to the sun) for orbital paths R083 and R126. Zeniths for both paths showed a seasonal wide range, varying from less than 25 degrees in mid-June to about 69 degrees in late December. The maximum difference between zenith angles for the two paths occurred in mid-June when zeniths for R083 were about a degree greater than for R126.

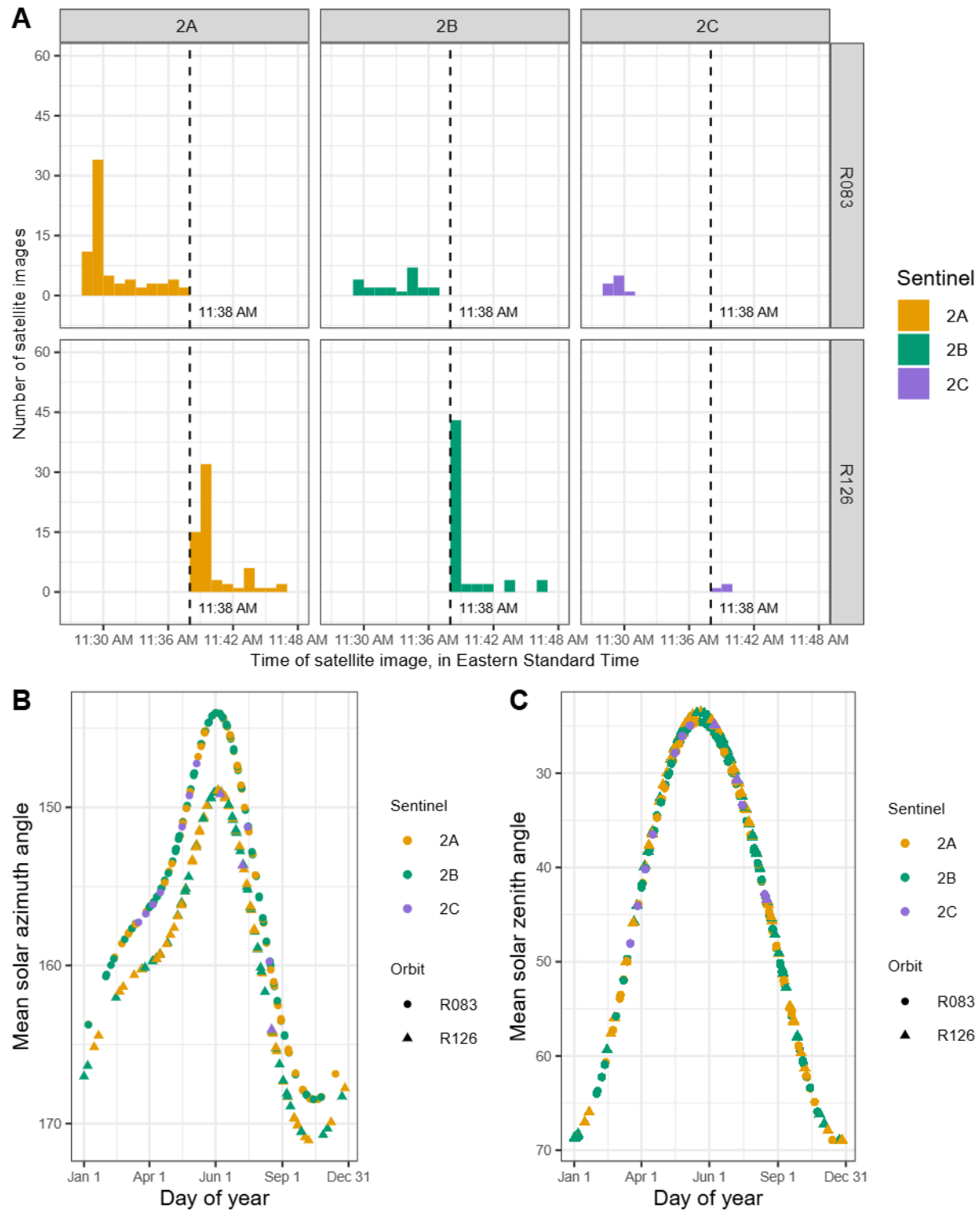


Figure 3. Solar azimuth and zenith angle of Sentinel-2 images for Torch Lake in Antrim County, Michigan

Once during the period from 2019 to 2025, Sentinel 2A and 2B captured a clear image of Torch Lake on the same day, April 11, 2025. The two images are of particular interest because changes in atmospheric transmission characteristics and wave conditions during the intervening 18 minutes and 22 seconds are thought to be minimal. This provides a basis for a better understanding the differences between orbit azimuth and zenith angles on reflectance characteristics.

The Sentinel 2A image was obtained at 16:47:01 UTC while in orbit R126, and Sentinel 2B captured an image at 16:28:39 UTC, while in orbit R083. The mean solar azimuth angles for satellites 2A and 2B were 159.59 and 155.67 degrees, and the mean solar zenith angles were 37.634 and 38.323, respectively. Thus, the Sentinel 2A perspective was about 4 degrees south-southwest of Sentinel 2B, with an elevation of less than 1 degree higher above the horizon.

Percent differences in surface reflectances  $_{[band]}\ddot{\mathcal{R}}_{[orbit]}$  for the blue, green, and red bands between images from orbits R083 and R126, were computed as:

$(_{[band]}\ddot{\mathcal{R}}_{R126} - _{[band]}\ddot{\mathcal{R}}_{R083}) / _{[band]}\ddot{\mathcal{R}}_{R083} \times 100$ . Figure 4 shows band-clustered boxplots of the differences between reflectances by orbit with increasing water-depth interval. For the blue band, these differences were consistently less than zero, with a decreasing means and increasing variabilities with increasing water-depth intervals. In contrast, mean red band differences were generally positive with generally increasing variability with water depth interval. Differences in green band reflectances were intermediate between blue and red bands, with mean differences appearing to differ little from zero.

The two Sentinel-2 acquisitions on April 11, 2025 (from different orbital paths) showed systematic reflectance differences by band that increased with water depth. These effects may be attributed to differences in atmospheric path length, and viewing geometry as indicated by differences in azimuth and zenith angles. An orbit-depth interaction term and a satellite factor term was included in the statistical models assess the statistical significance of these effects.

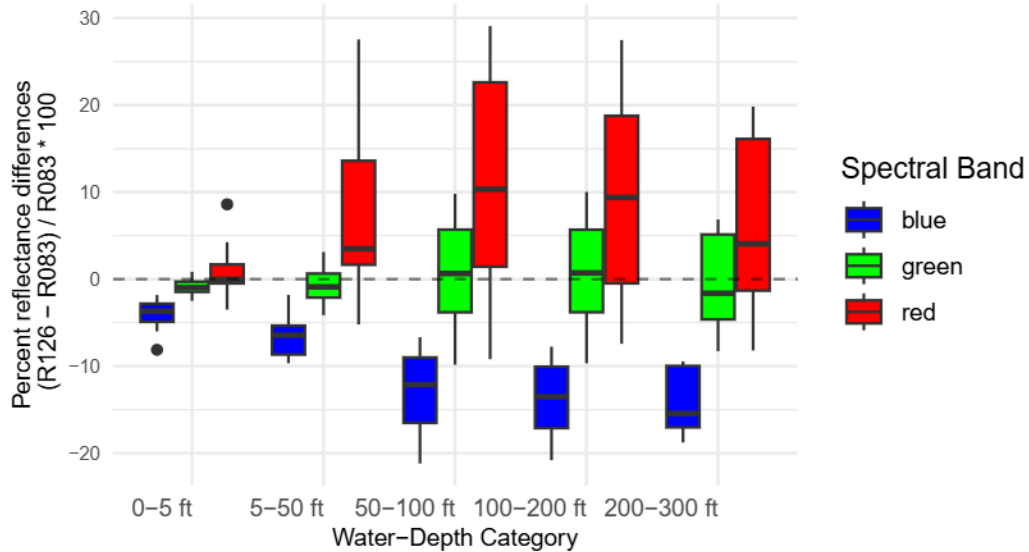


Figure 4. Differences between reflectances of blue, green, and red light from Torch Lake obtained by Sentinel 2A and 2B satellites on April 11, 2025 by color band and water-depth interval

### Horizontal Masking and Stratification of Torch Lake

Within the Torch Lake, a 30-m buffer was extended from the lake boundary (edge of water) inward towards the center of the lake. This buffered area was masked to exclude reflectances from overhanging trees, docks, and other features that would not have the same reflectance properties as water near the shoreline.

The unmasked surface area of Torch Lake was then subdivided into 60 strata by crossing 5 water-depth intervals (0-5, 5-50, 50-100, 100-200, 200-300 ft) with northing and easting extents. Torch Lake was partitioned longitudinally into eastern and western basins by a north-south section through the center of the lake. Then, five transverse sections, at approximately equal intervals, subdivided the lake again into six subbasins, in which the east-west basins were again partitioned into north, central, and south subbasins.

Figure 5 shows how the 60 strata were labelled with an alphanumeric character string of length four. The first character indicates the lake basin as north (N) or south (S). The second character represents subbasins in which two transverse lines subdivided each basin into northern (N), central (C), and southern (S) subbasins. The final numeric character corresponds to water-depth interval, where 1 is 0-5 ft. A central point lying within each strata was identified to compute the distances between strata centroids based on isotropic coordinates expressed in northings and eastings, rather than latitudes and longitudes (table 1).

Each satellite image of Torch Lake can measure surface reflectances from 737,159 10-m by 10-m pixels, ranging by strata from 1,256 pixels to 37,113 pixels, depending on their surface areas (Appendix table 1). The median reflectance was selected as a robust statistic to describe individual strata reflectances. The location of the median pixel within each strata is not known for every satellite image, so median pixels were assigned to a fixed position at the centroid of the strata. Distances between centroids were then used to characterize possible spatial correlations between model errors to account for redundancies in measured reflectances.

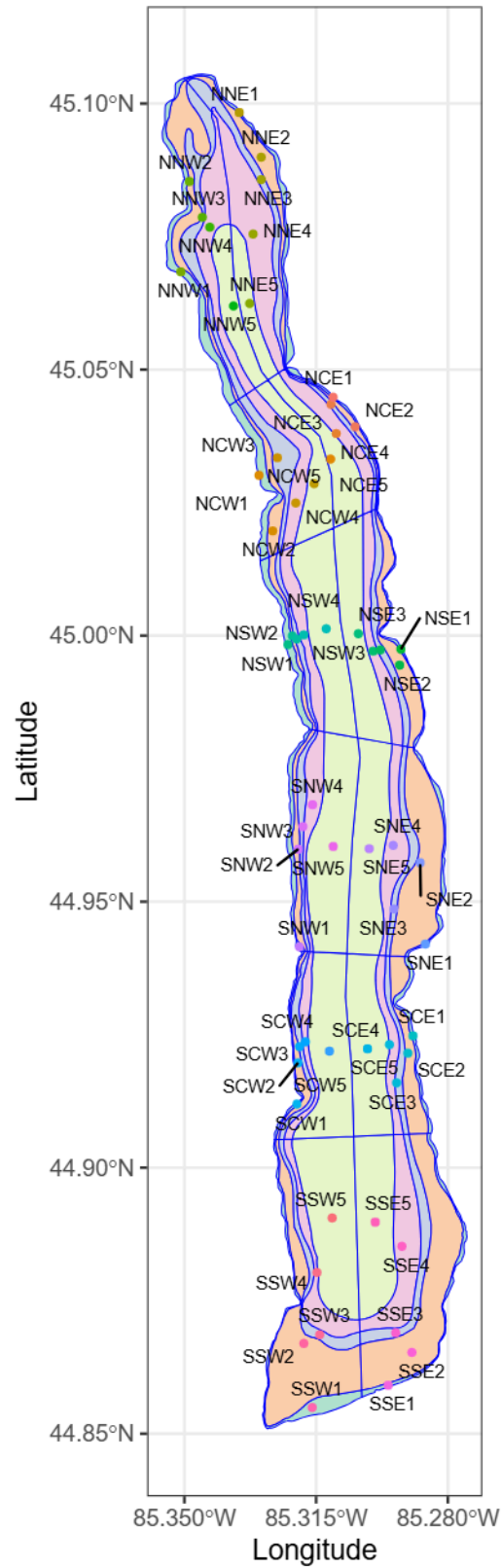


Figure 5. Torch Lake with 60 subbasins and the central points of each subbasin polygon in Antrim County, Michigan

### Statistical Distribution of Reflectances

The left pane of figure 6 shows the empirical cumulative distribution function for Sentinel 2 surface reflectances  $\mathcal{R}$  from Torch Lake by band and water-depth interval. The distribution of reflectances at water-depth intervals greater than 50-ft were similar, and that these reflection intensities were generally lower (darker) than intensities are shallower depths. The reflection intensities for all bands were greatest at the 0-5 ft depth interval. Note that for all bands and water-depth intervals the cumulative probability approaches 1 at a median reflectance intensity of about 0.2, implying that few values were greater than 0.2. To avoid outliers, the  $\mathcal{R}$  used in this analysis were limited to intensities with the  $[0, 0.2]$ , forming  $\hat{\mathcal{R}}$ .

The right pane of figure 6 shows the empirical probability density by band and water-depth interval. At shallower depths, maximum reflectance intensities are in green band, while at water-depth intervals greater than 50-ft the greatest reflectance intensities occur in the blue band. The red band has lower peak intensities for all water-depth intervals than the blue or green bands. Note the x-axis reflects a square-root transformation, which was applied to help normalize the distribution of reflectance intensities forming  $\hat{\mathcal{R}}$ . Normalizing the distribution of the reflection intensities improves the likelihood that model errors will be normally distributed, which is explicitly assumed in the modelling approach.

### Time Series of Reflectance Data

Figures 7 and 8 show time series of reflectances for the blue, green, and red bands from the northern and southern subbasins grouped into strata of Torch Lake. Columns show data for progressively increasing water-depth intervals, with the left-most column showing data for water depths of 0-5 ft and the right-most column showing data for water depths of 200-300 ft. Note that the reflectance intensities in the 0-5 ft intervals are generally higher for all bands and depths. Adjacent rows are grouped into three pairs showing data for the upper, middle, and lower strata within each the northern and southern basins, respectively. The paired rows contain data for strata on the western and eastern sides of a midline that longitudinally bisects Torch lake. Seasonal patterns are apparent in the fluctuations of reflectance intensities for all bands and water-depth intervals. There is some visual indications that a positive trend may be present in the data. Note that a square-root transformation was applied to the y-axis and to the corresponding trimmed reflectances values  $\hat{\mathcal{R}}$  to provide the transformed reflectances  $\tilde{\mathcal{R}}$  used in model development.

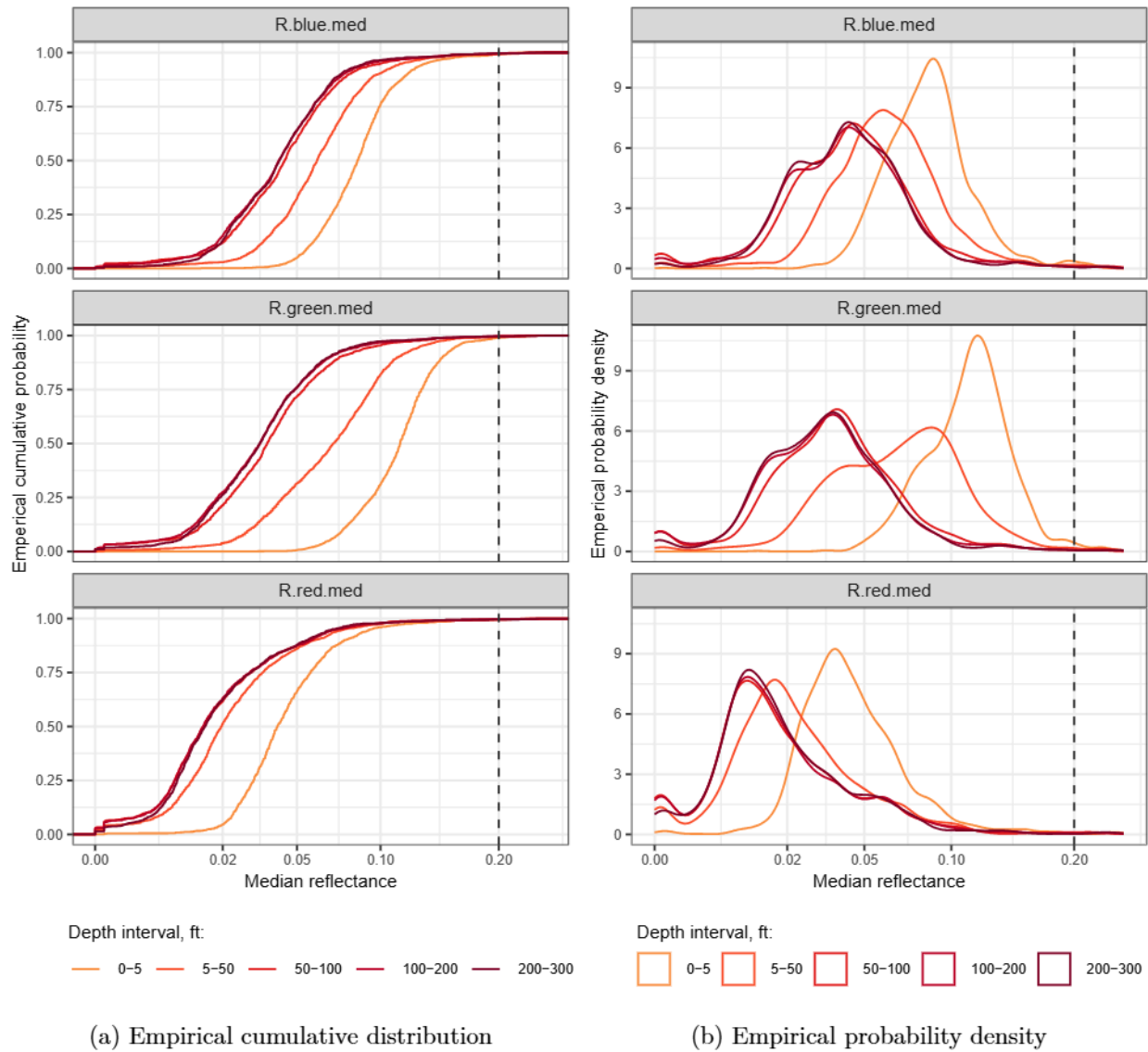


Figure 6. Median surface reflectances of Sentinel 2 data from Torch Lake by water-depth interval and color band

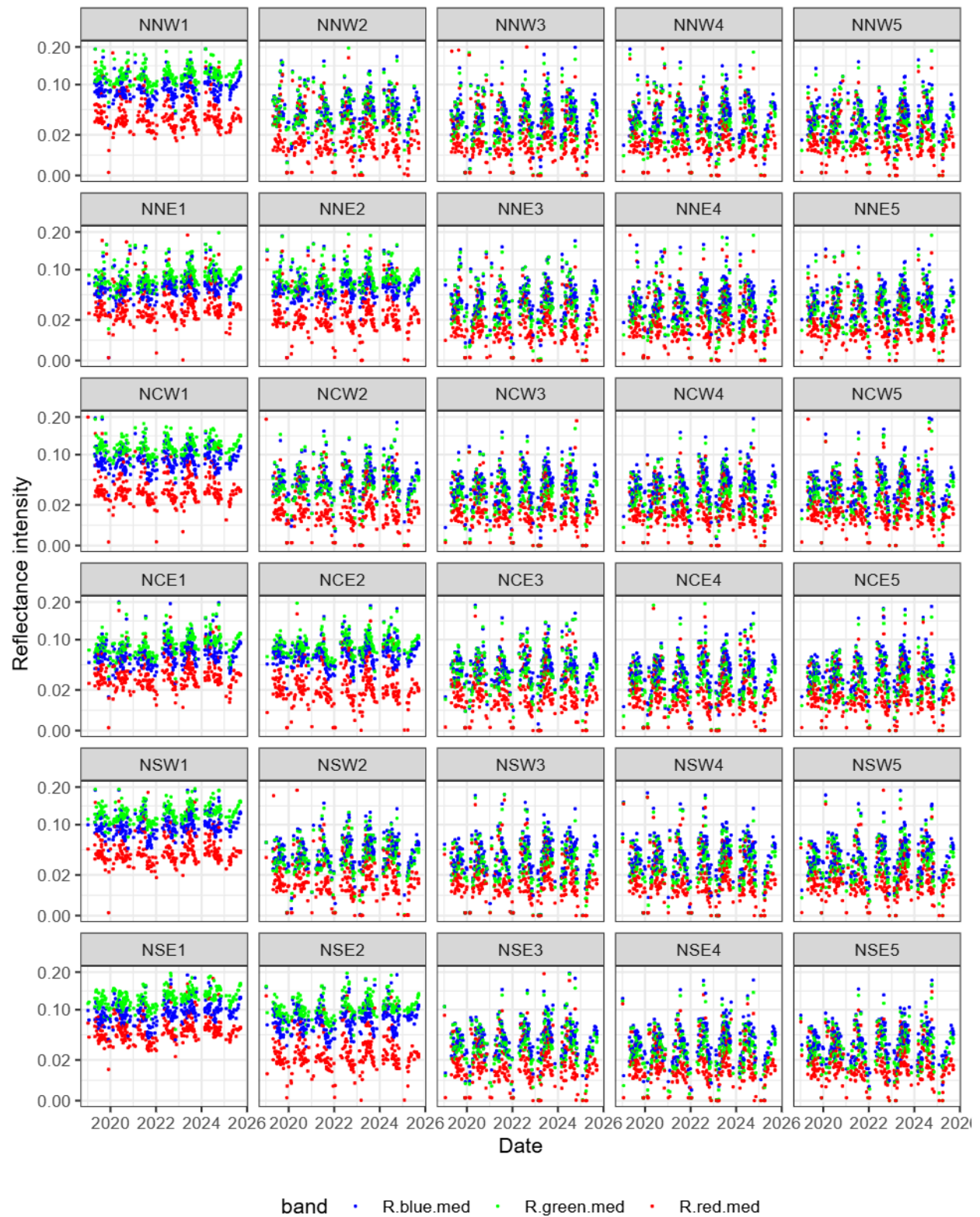


Figure 7. Time-series plots of blue, green, and red surface reflectances from all northern strata in Torch Lake, Antrim County, Michigan

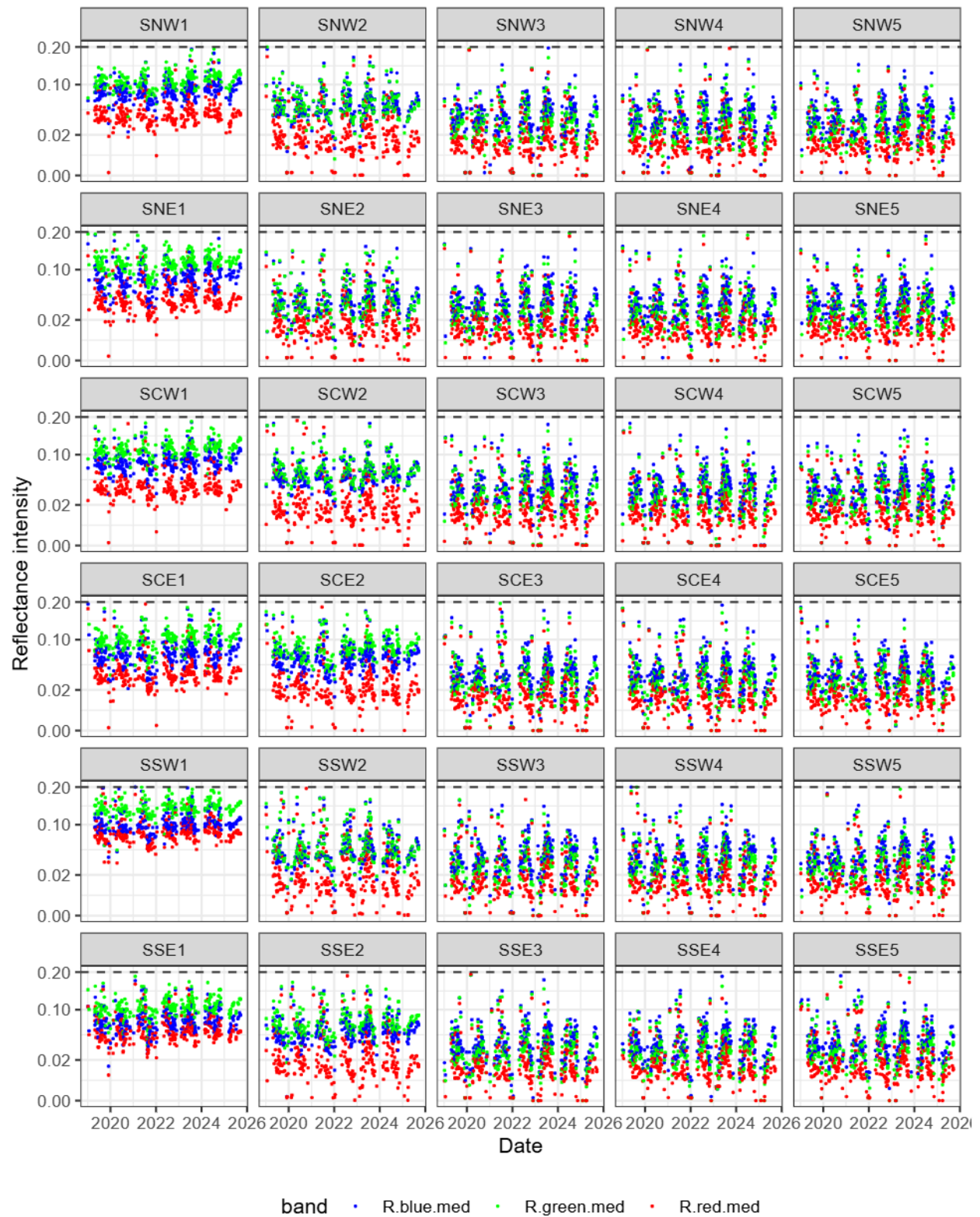


Figure 8. Time-series plots of blue, green, and red surface reflectances from all southern strata in Torch Lake, Antrim County, Michigan

## Statistical Modeling Approach

A statistical modeling approach is used to characterize the median surface reflectances from Torch Lake in the blue, green, and red bands of visible light from Sentinel-2 imagery and ancillary data. The modeling approach identifies and estimates systematic variations of reflectances associated with fixed and smooth components, compensating for temporal or spatial anomalies with random intercepts, and modeling correlations in model errors to reduce the effect of measurement redundancy.

### Modeling Framework

Models were developed using The R Language and Environment for Statistical Computing (R Core Team 2025a) in the RStudio integrated development environment (R Core Team 2025b). The `quarto` markdown publishing system (Allaire and Dervieux 2024) was used to prepare a portable document formatted (PDF) file in Latex output. The `mgcv` package (Wood 2017) was used to develop the generalized additive model (GAM) and the generalized additive mixed-effect models (GAMM). Figures included in the report were generally prepared with the `ggplot2` package (Wickham 2016).

The GAM model provides a flexible approach for including both fixed and smooth components in the analysis of surface reflectance from satellite data Holschlag (2024). There are two difficulties, however, that are not addressed by this model structure. First, the reflectance measured by a satellite is a function of more than one independent random processes that include the reflective properties of the lake surface itself, and (2) the light transmission characteristics of the atmosphere through which the light passes. Although much productive effort is expended by the ESA and similar agencies to provide corrections from top of atmosphere (TOA) satellite measurements to provide estimates of surface reflectance or bottom of the atmosphere (BOA). Still, atmospheric corrections are imperfect. Second, due to the stratification of Torch Lake into 60 subbasins, and frequent repetitive measurements, spatial and temporal correlations of measurement errors may be introduced. Without accounting for these correlations, the statistical significance of parameter estimates may be overestimated.

Extension to a GAMM model provides two model components: (1) a GAM component to estimate fixed and smooth effects, and (2) a linear mixed effect (LME) component to account for random effects and error correlation. A random component can be specified to model the random temporal errors in atmospheric corrections and a model to characterize spatial random differences between mean strata reflectances. This random component could take the form of a set of random intercepts that are independent and normally distributed about zero with an estimated standard deviation. Similarly, a temporal or spatial correlation function could be estimated of model errors to properly adjust the effective number of satellite measurements.

### Modeling Equation

Equation 1 shows the full form of the generalized additive mixed-effect models (GAMM) estimated in this analysis.

$$\begin{aligned} \lambda \ddot{\mathcal{R}}_{s_i, t_k} = & \hat{\beta}_1 + \sum_{j=2}^5 I(s_{\{i\}} = \text{depth}_j) \hat{\beta}_j + I(\text{orbit}_{t_k}) \hat{\beta}_6 + \delta \text{Day}_k \hat{\beta}_7 \\ & + f_1\left(\sqrt{1 - \text{cloud.score}_{s_i, t_k}}\right) + f_2\left(\text{day.of.year}_{\{t_k\}}, \text{by} = \text{depth}_j\right) + \vec{\mathbf{b}} + \epsilon_{s_i, t_k} \end{aligned} \quad (1)$$

where:

$\ddot{R}_{s_i, t_k}$  are measures of reflectances in blue, green, and red bands for strata  $s_i$  at time  $t_k$ , where the distribution of measured reflectances were trimmed to reduce outliers and square-root transformed to normalize their distribution,

$\hat{\beta}_1$  is the estimated intercept term. Note all terms that include a  $\beta$  parameter are associated with fixed effects,

$I(s_{\{i\}} = \text{depth}_j)$  are factor indicators ( $I$ ) of reflectances in all 12 strata within each of 5 water-depth intervals [0-5, 5-50-, 50-100, 100-200, and 200-300] ft spanning Torch Lake. The indicators are treated as ordered factor variables referenced to the 0-5 ft depth interval, which results in a  $\beta = 0$  for the first water-depth interval, and is therefore not estimated,

$I(\text{orbit}_{t_k})$  are factor indicators of the satellite orbit, with 0 corresponding to reference orbit R083, and  $\hat{\beta}_6$  the difference between reflectances for orbits R083 R126,

$\delta \text{Day}_k$  is the number of days since Jan. 6, 2019, and  $\hat{\beta}_7$  is the estimate of linear trend,

$f_1\left(\sqrt{1 - \text{cloud.score}_{s_i, t_k}}\right)$  uses  $f_2$  to describe the relation between the Google's Cloud Score+ index and reflectance. The index ranges from 0 to 1, where 0 indicates "not clear" (occluded), and 1 indicates "clear". The index is used to remove pixels that are affected by clouds or cloud shadows from a satellite image,

$f_2\left(\text{day.of.year}_k, \text{by} = \text{depth}_j\right)$  is the smooth that describes the seasonality of reflectance by water-depth interval by use of the day of year (day.of.year), in which January 1 corresponds to 1 of 365 days,

$\vec{\mathbf{b}}$  when this vector of random-effect intercepts is included in an estimated model, they are associated with either strata to characterize spatial random variations, or with **Days** to characterize temporal random variations. Although error correlations between strata and between temporal measurements likely occurs, only one component can be estimated. associated with or time  $t_k$  such that  $\vec{\mathbf{b}} \sim \mathcal{N}(\vec{0}, \psi_\theta)$  where  $\psi_\theta$  is an estimated covariance of random intercepts, and

$\epsilon_{s_i, t_k}$  denotes the model residual for stratum  $s_i$  at time  $t_k$ , which may have an estimated spatial or temporal covariance structure such that  $\epsilon_{s_i, t_k} \sim \mathcal{N}_{\mathcal{J}\mathcal{J}\mathcal{D}}(\vec{0}, \Lambda\sigma^2)$ , where  $\mathcal{N}_{\mathcal{J}\mathcal{J}\mathcal{D}}$  indicates that the model errors  $\epsilon_{s_i, t_k}$  are for Normal, Independent, and Identically Distributed.

## Model Specifications

Four different forms of generalized additive models were estimated for each of three color bands developed in the analysis. In table 3, the model form is identified by the first digit of the model 'ID' column. Other characters in the ID string reflect the Band [b,g,r], Model [GAM, GAMM], correlation [None, Temporal, Spatial], and random component [None, strata,  $\delta$ Days], respectively.

Model 1 is a Generalized Additive Model (GAM) that models only fixed effects and smooth terms. It is basically the form of the model used by Holschlag (2024) to model surface-reflectance data from Torch Lake using imagery from the Landsat 5-9 satellites. Note that 60 strata were used in the present analysis, rather than 10 strata used previously. Model 2 includes the same components as Model 1, but is estimated using the Generalized Additive Mixed-Effects Model (GAMM), which has somewhat different numerical estimation algorithms. Model 3 is also a GAMM but includes a random integer component for strata and a temporal correlation structure. Model 4 is a GAMM model having the same fixed and smooth components models 1-3, but includes a random intercept component for temporal variations, and a spatial correlation structure based on separation distance between strata centroids. The response variables for all models are the square root of scaled and trimmed reflectance values for the corresponding band.

### Model Selection Criteria

In this report, the key statistics used for model selection are the coefficient of determination ( $R^2$ ), the root-mean-square-error (RMSE), and two information-theoretic based criteria. Both the  $R^2$  and RMSE values provide an estimation error that describes how well the model fits the data used in model development. The  $R^2$  value is the ratio of the variances of predicted and measured reflectances  $var(\hat{R})/var(\ddot{R})$ . The RMSE is the standard deviation of model residuals  $\sqrt{(\sum(\ddot{R} - \hat{R})^2)/(n - p)}$ , where  $n$  is the number of observations and  $p$  is the number of parameters. Both of these metrics provide intuitive means for characterizing model estimation error. A difficulty arises, however, in comparing models with differing complexities (number of parameters), as a more complex model may attain a higher  $R^2$  and lower RMSE on the estimation data set by over-fitting the data, but may not perform as well on a new data set drawn from the same population used for prediction.

Information-theoretic based criteria for model selection, like Akaike information criterion (AIC equation 2) and the Bayesian information criterion (BIC equation 3) provide alternative estimators that penalize model estimation performance for model complexity. This is achieved by including terms that increase with the number of estimated parameters  $p$  and decrease with the goodness of fit, as assessed by the maximum value of the likelihood function.

$$AIC = 2p - 2 \max_{\theta} \log \widehat{Lik}(\theta) \quad (2)$$

$$BIC = p \cdot \log(n) - 2 \max_{\theta} \log \widehat{Lik}(\theta) \quad (3)$$

where:

$AIC$  is the Akaike Information Criteria,

$BIC$  is the Bayesian Information Criteria,

$p$  is the number of estimated parameters in  $\hat{\theta}$ ,

$\max_{\theta} \log \widehat{Lik}(\hat{\theta})$  is the logarithm of the estimated maximum likelihood function at  $\hat{\theta}$ , and

$n$  is the number of observations.

When selecting among alternative models, the model with the minimum AIC or BIC value is generally preferred. With AIC, the penalty for  $p$  parameters is  $2p$ , while the BIC penalty is

generally larger at  $\log(n) \cdot p$ , where  $n$  is the number of observations in the data set. In particular, the number of observations in this analysis was 15,690, with  $\log(15690) = 9.66 \gg 2$ . So, the BIC statistics was preferred to provide a greater penalty for increased complexity.

When comparing two models,  $m1$  and  $m2$ , with BIC statistics of  $BIC_{m1} < BIC_{m2}$ , the relative likelihood that  $m2$  minimizes information loss with respect to  $m1$  is:

$$\text{Relative likelihood} = \frac{Like_{m2}}{Like_{m1}} \approx \exp\left(\frac{BIC_{m1} - BIC_{m2}}{2}\right) \quad (4)$$

For example, a  $BIC_{m1} = 0$  and  $BIC_{m2} = 10$ , would produce a ( $\Delta BIC = -10$ ), which indicates that the relative likelihood that  $m2$  minimizes information loss is proportional to 0.007. In contrast, a smaller difference as of -2 indicates that  $m2$  is 0.368 times as probable to minimize information loss as  $m1$ . The relative likelihood approximation (equation 4) is accurate as long as  $k_1 \approx k_2$  and  $n_1 \approx n_2$ .

## Model Selection

Table 3 shows summary statistics for model selection. Models are identified by two sets of strings separated by ‘.’ in the column labelled ‘ID’. The first set contains elements labelled {1,2,3,4} corresponding to the model structure. The model structure includes the model type (GAM or GAMM), the correlation structure of model errors (None, Temporal, Spatial), and the random effect specified (None, strata,  $\delta$ Days). The second set contains {b,g,r} corresponding to three visible light bands of blue, green, red.

Model 4 was selected to characterize fixed effects associated with water-depth intervals and orbit, smooths associated with time ( $\delta$ Days), the square root of 1 - cloud score (one.cloud.score.sqrt), and seasonal variation with day of year by water-depth interval (s(day.of.year):depth). In addition, the spatial correlation of model errors between strata centroids was estimated, and random intercept effects are computed for days of selected images.

The selection is consistent with minimizing the RMSE and BIC statistics discussed above. In particular, model 4 had 4.1- to 17.3-percent lower RMSE values compared with model 3, which was consistently the model with the next lowest RMSE values for all color bands. Similarly, the BIC statistics for model 4 were lower than other three models. Specifically, the relative likelihoods that models 1, 2, or 3 would minimize the information loss relative to model 4 is essentially 0 based on  $\Delta BICs$  that were sometimes less than -10,000. Within the same bands, the  $R^2$  values for models 1-3 were nearly identical, and averaged 2.8 percent higher than the  $R^2$  values for model 4. Models 1 and 2 had nearly identical RMSE and  $R^2$  values for all bands, although relative likelihoods favored model 2 relative to model 1 based on  $\Delta BICs$ .

The inclusion of a spatial correlation component in the selected model necessitates the specification of the form of the correlation model. The mgcv package (Wood 2017) includes six forms considered in this analysis. For each band investigated, the exponential decay model (corExp) was ranked first with the lowest BIC among alternative correlation models (table 2) is consistent with GAMM ID4.

Table 2. Comparison of GAMM ID4 BIC fit statistics for alternative spatial correlation functions

Structure	Function	BIC	Rank
Blue band			
Exponential	corExp()	-70,770	1
Spherical	corSpher()	-69,874	2
Linear	corLin()	-69,413	3
Rational quadratic	corRatio()	-69,177	4
Gaussian	corGaus()	-67,424	5
None	- -	-66,934	6
Green band			
Exponential	corExp()	-63,415	1
Spherical	corSpher()	-62,431	3
Linear	corLin()	-62,281	4
Rational quadratic	corRatio()	-62,915	2
Gaussian	corGaus()	-62,275	5
None	- -	-62,168	6
Red band			
Exponential	corExp()	-71,796	1
Spherical	corSpher()	-70,881	2
Linear	corLin()	-70,017	3
Rational quadratic	corRatio()	-68,770	4
Gaussian	corGaus()	-65,916	5
None	- -	-63,248	6

Note:

Spatial correlation = cor[Function](form = ~ East\_migeoref83.km + Nrth\_migeoref83.km

Table 3. Comparison of alternative GAMM forms to estimate surface reflectance from Torch Lake in Antrim County, Michigan

ID	Band	Model	Correlation	Random	RMSE	R2	logLik	BIC	Correlation	Random Effect
			Structure	Component					Range	SD(Intercept)
1.b	Blue	GAM	None	None	0.0411	0.6410	29837.	-59084.	—	—
2.b		GAMM	None	None	0.0411	0.6409	29715.	-59226.	—	—
3.b		GAMM	Temporal	strata	0.0391	0.6404	30563.	-60903.	1.8768	0.0126
4.b		GAMM	Spatial	$\delta$ Days	<u>0.0321</u>	<u>0.6289</u>	35497.	<u>-70770.</u>	0.9216	0.0234
1.g	Green	GAM	None	None	0.0439	0.7440	28728.	-56866.	—	—
2.g		GAMM	None	None	0.0439	0.7439	28607.	-57009.	—	—
3.g		GAMM	Temporal	strata	0.0390	0.7437	30563.	-60902.	1.7122	0.0204
4.g		GAMM	Spatial	$\delta$ Days	<u>0.0370</u>	<u>0.7344</u>	31820.	<u>-63415.</u>	0.5677	0.0223
1.r	Red	GAM	None	None	0.0455	0.6212	28127.	-55666.	—	—
2.r		GAMM	None	None	0.0455	0.6210	28010.	-55816.	—	—
3.r		GAMM	Temporal	strata	0.0436	0.6211	28616.	-57009.	0.6347	0.0129
4.r		GAMM	Spatial	$\delta$ Days	<u>0.0369</u>	<u>0.6065</u>	36010.	<u>-71796.</u>	1.8563	0.0210

<sup>1</sup> Model options: GAM (Generalized Additive Model), GAMM (Generalized Additive Mixed-effect Model),<sup>2</sup> RMSE is the root mean square error of the model deviations,<sup>3</sup> R2 is the coefficient of determination,<sup>4</sup> logLik is the maximized value of the log likelihood function,<sup>5</sup> AIC is the Akaike Information Criterion,<sup>6</sup> BIC is the Bayesian Information Criterion,<sup>7</sup> Range is the length of the correlation structure, in days or kilometers<sup>8</sup> SD(Intercept) is the standard deviation of the random intercepts, and<sup>9</sup> The number of observations in all models is about 15,690, but varies slightly among bands for NA values.

## Discussion

### Fixed Effects Associated with Water-Depth Intervals, Satellite Orbit, and Trend

Table 4 shows the fixed-effect parameters for GAMM ID4. Water-depth interval *depth* is a factor variable with five ordered levels. The 0-5 ft interval is the reference level, which is not explicitly estimated but defaults to parameter estimates of zero. This enables comparison of statistical significance of estimated parameters for other water depth intervals relative to the 0-5 ft interval. This convention also allows estimation of the model intercept.

The *depth* parameter estimates for all bands generally decrease with greater water depths, although within-band variations of parameters for water-depth intervals greater than 50-ft show little variation. The negative parameter values imply that reflectances decrease with water depths. The satellite orbit is a factor variable with two ordered levels R083 and R126, where R083 is the reference level. Parameter estimates indicate that reflectances for all bands are greater for orbit:R126. Finally, the variable *deltaDays* ( $\delta Days$ ) is the number of days since Jan. 6, 2019, the date of the first image used in this analysis. The positive valued parameters indicate a slightly positive linear trend for all bands.

Table 4. Fixed effect terms for band reflectances from Torch Lake in Antrim County, Michigan

Band	Water-depth intervals, ft	Parameter estimates	Standard errors	t-values	p-values
Blue	(Intercept)	2.610e-01	3.905e-03	66.826	<2e-16
	orbit R126	6.389e-03	3.218e-03	1.985	4.71e-02
	depth 5-50	-3.740e-02	7.562e-04	-49.463	<2e-16
	depth 50-100	-8.760e-02	7.129e-04	-122.885	<2e-16
	depth 100-200	-9.085e-02	8.126e-04	-111.801	<2e-16
	depth 200-300	-8.742e-02	9.877e-04	-88.508	<2e-16
	SAT 2B	8.827e-03	3.164e-03	2.790	5.28e-03
	SAT 2C	-3.947e-03	8.460e-03	-0.467	6.41e-01
	deltaDays	1.284e-05	2.453e-06	5.234	1.68e-07
	orbit R126:depth 5-50	5.116e-03	1.152e-03	4.440	9.05e-06
	orbit R126:depth 50-100	1.250e-02	1.087e-03	11.505	<2e-16
	orbit R126:depth 100-200	1.355e-02	1.239e-03	10.942	<2e-16
	orbit R126:depth 200-300	1.270e-02	1.506e-03	8.434	<2e-16
Green	(Intercept)	3.120e-01	3.717e-03	83.924	<2e-16
	orbit R126	5.124e-03	3.119e-03	1.643	1e-01
	depth 5-50	-6.825e-02	1.009e-03	-67.616	<2e-16
	depth 50-100	-1.535e-01	9.531e-04	-161.050	<2e-16
	depth 100-200	-1.592e-01	1.056e-03	-150.780	<2e-16
	depth 200-300	-1.543e-01	1.224e-03	-126.048	<2e-16
	SAT 2B	-7.340e-04	2.993e-03	-0.245	0e+00
	SAT 2C	-1.023e-02	7.964e-03	-1.285	1e-01
	deltaDays	1.015e-05	2.314e-06	4.387	0e+00
	orbit R126:depth 5-50	7.342e-03	1.537e-03	4.778	0e+00
	orbit R126:depth 50-100	1.876e-02	1.452e-03	12.919	<2e-16
	orbit R126:depth 100-200	1.976e-02	1.609e-03	12.279	<2e-16
	orbit R126:depth 200-300	1.882e-02	1.865e-03	10.092	<2e-16
Red	(Intercept)	2.023e-01	4.135e-03	48.93	<2e-16
	orbit R126	1.160e-02	3.392e-03	3.42	6.28e-04
	depth 5-50	-6.591e-02	6.740e-04	-97.78	<2e-16
	depth 50-100	-8.748e-02	6.376e-04	-137.19	<2e-16
	depth 100-200	-8.838e-02	7.460e-04	-118.46	<2e-16
	depth 200-300	-8.522e-02	9.394e-04	-90.71	<2e-16
	SAT 2B	-2.895e-03	3.365e-03	-0.86	3.90e-01
	SAT 2C	-1.436e-02	8.970e-03	-1.60	1.10e-01
	deltaDays	6.115e-06	2.605e-06	2.35	1.89e-02
	orbit R126:depth 5-50	1.282e-02	1.027e-03	12.48	<2e-16
	orbit R126:depth 50-100	1.757e-02	9.719e-04	18.08	<2e-16
	orbit R126:depth 100-200	1.854e-02	1.137e-03	16.30	<2e-16
	orbit R126:depth 200-300	1.732e-02	1.432e-03	12.10	<2e-16

## Smooth Effects Describing Seasonal Variations by Depth and Cloud Score Associations

Table 5 shows a smooth term associated with the variable `one.cloud.score.sqrt` and a smooth term approximating the seasonal component for each water-depth interval using the variable `day.of.year`. Note that the effective and reference degrees of freedom for  $s(\text{one.cloud.score.sqrt})$  are equal for each band, while the effective degrees of freedom are generally less than the reference degrees of freedom for all  $s(\text{day.of.year} : \text{depth})$  intervals. Also, the F-statistics for  $s(\text{one.cloud.score.sqrt})$  are similar in magnitude between bands. The F-statistics for the blue and green bands are generally greater than red band for water-depth intervals greater than 50-ft. Finally, the  $p$  – values for all but one smooth component indicates high statistical significance for the smooth components.

Table 5. Smooth terms from GAMM for Sentinel 2 band reflectances from Torch Lake in Antrim County, Michigan

Band	Smooths	Degrees of freedom		F-statistics	p-values
		Effective	Reference		
Blue	$s(\text{one.cloud.score.sqrt})$	2.9733	2.9733	124.0569	<2.0000e-16
	$s(\text{day.of.year}:\text{depth } 0\text{-}5)$	6.2938	8.0000	5.0992	<2.0000e-16
	$s(\text{day.of.year}:\text{depth } 5\text{-}50)$	3.2509	8.0000	2.2461	3.0437e-05
	$s(\text{day.of.year}:\text{depth } 50\text{-}100)$	7.3288	8.0000	48.7539	<2.0000e-16
	$s(\text{day.of.year}:\text{depth } 100\text{-}200)$	7.3141	8.0000	45.3552	<2.0000e-16
	$s(\text{day.of.year}:\text{depth } 200\text{-}300)$	7.1206	8.0000	31.3999	<2.0000e-16
Green	$s(\text{one.cloud.score.sqrt})$	3.3952	3.3952	121.9434	<2.0000e-16
	$s(\text{day.of.year}:\text{depth } 0\text{-}5)$	9.6213e-06	8.0000	5.4262e-07	0.6127
	$s(\text{day.of.year}:\text{depth } 5\text{-}50)$	4.5522	8.0000	18.9180	<2.0000e-16
	$s(\text{day.of.year}:\text{depth } 50\text{-}100)$	7.2882	8.0000	224.8581	<2.0000e-16
	$s(\text{day.of.year}:\text{depth } 100\text{-}200)$	7.2391	8.0000	181.7990	<2.0000e-16
	$s(\text{day.of.year}:\text{depth } 200\text{-}300)$	6.9059	8.0000	96.8710	<2.0000e-16
Red	$s(\text{one.cloud.score.sqrt})$	4.3523	4.3523	112.9326	<2.0000e-16
	$s(\text{day.of.year}:\text{depth } 0\text{-}5)$	6.5717	8.0000	7.1780	<2.0000e-16
	$s(\text{day.of.year}:\text{depth } 5\text{-}50)$	5.0074	8.0000	5.4666	<2.0000e-16
	$s(\text{day.of.year}:\text{depth } 50\text{-}100)$	6.0009	8.0000	9.0568	<2.0000e-16
	$s(\text{day.of.year}:\text{depth } 100\text{-}200)$	5.8192	8.0000	7.7458	<2.0000e-16
	$s(\text{day.of.year}:\text{depth } 200\text{-}300)$	4.7108	8.0000	4.4812	<2.0000e-16

Figure 9 shows the monotonic increase in reflectance intensity deviances over the range of  $\text{one.cloud.score.sqrt}$  using the square-root function to help reduce the skewness of the explanatory variable  $\sqrt{1 - \text{cloudScore}}$ . Note that the 95-percent confidence intervals commonly contain the estimates for all bands indicating little difference in cloud score effects among bands.

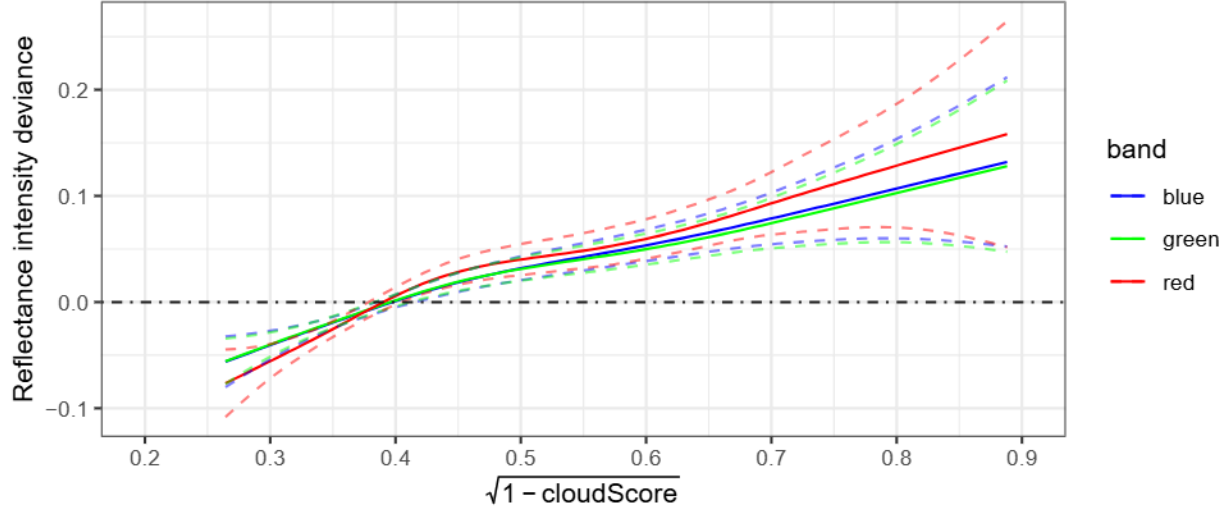


Figure 9. Variation of reflectance intensity with cloud score

Figure 10 shows GAMM ID4 estimated seasonal component of band reflectance by water-depth interval for Sentinel 2 data obtained between 2019 and 2025. The 0-5 and 5-50 ft intervals show minor seasonal variations while considerable seasonal variations are evident at water-depth intervals greater than 50 ft. The seasonal variations among bands are similar at water-depth intervals greater than 50 ft. The 0-5 ft water-depth interval may be more indicative of reflectances in the benthic areas and variations at water-depth intervals greater than 50 ft may be more indicative of reflectances in the water column.

Figure 11 shows the GAM estimated seasonal variation reported by Holtschlag (2024) using Landsat data from 1984 to 2023. Similarities include peaks in the blue and green band reflectances near the first week of September at water-depth intervals greater than 50-ft. Also, the amplitudes of seasonal variations were generally lower at water-depth intervals less than 50-ft. The most conspicuous differences in reflectances occur in the red band that are generally concave down for water-depth intervals greater than 50-ft in Sentinel 2 data and concave up for Landsat data.

Figures 12 and 13 show true-color composite images from Sentinel 2 data for the weeks of April 10, July 9, September 7, and December 1. In the composites are based on the highest quality pixels (least cloud affected) for each specified week based on the period of record (2019-2025). The series highlights the seasonal changes in measured reflectances.

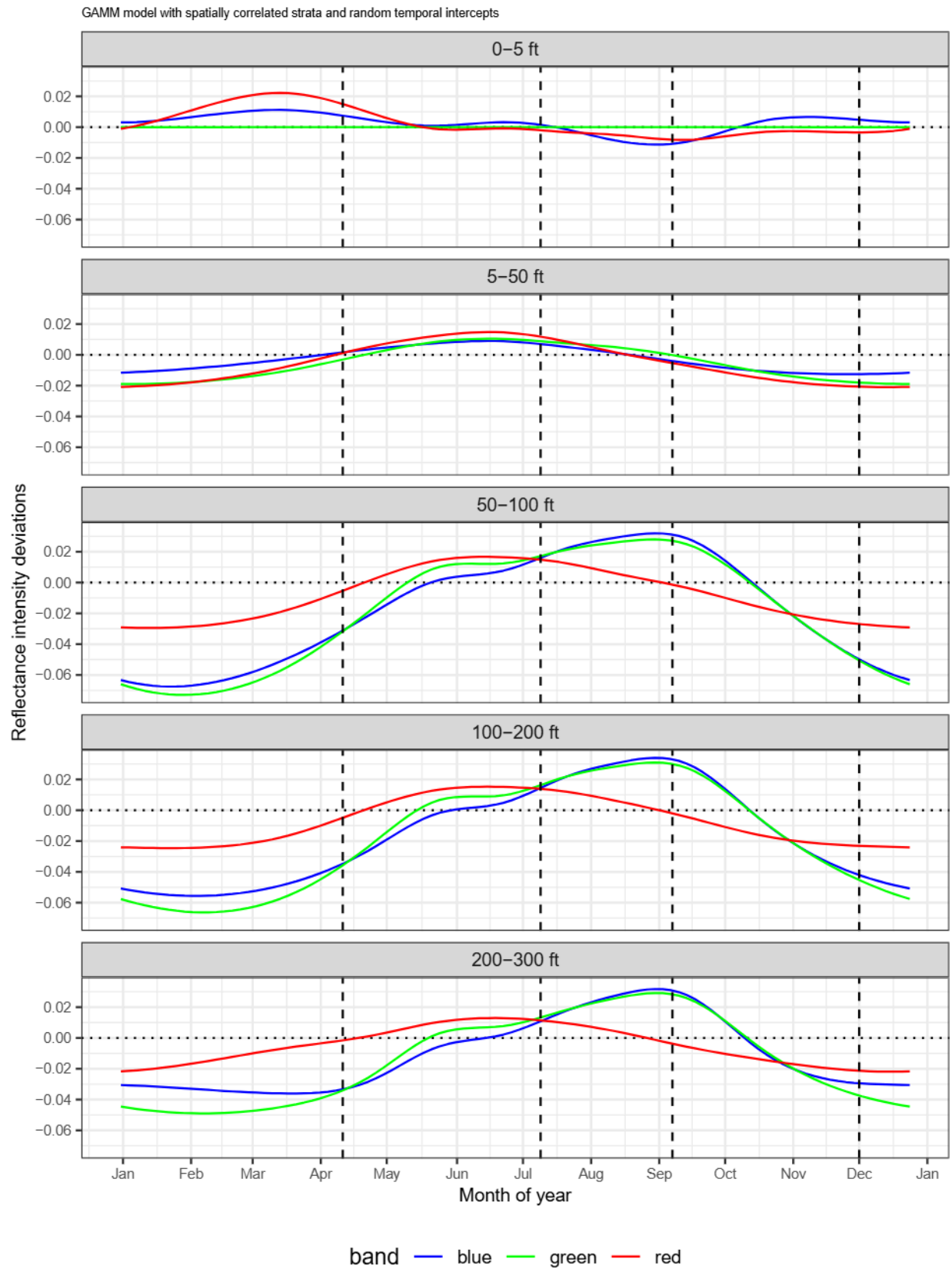
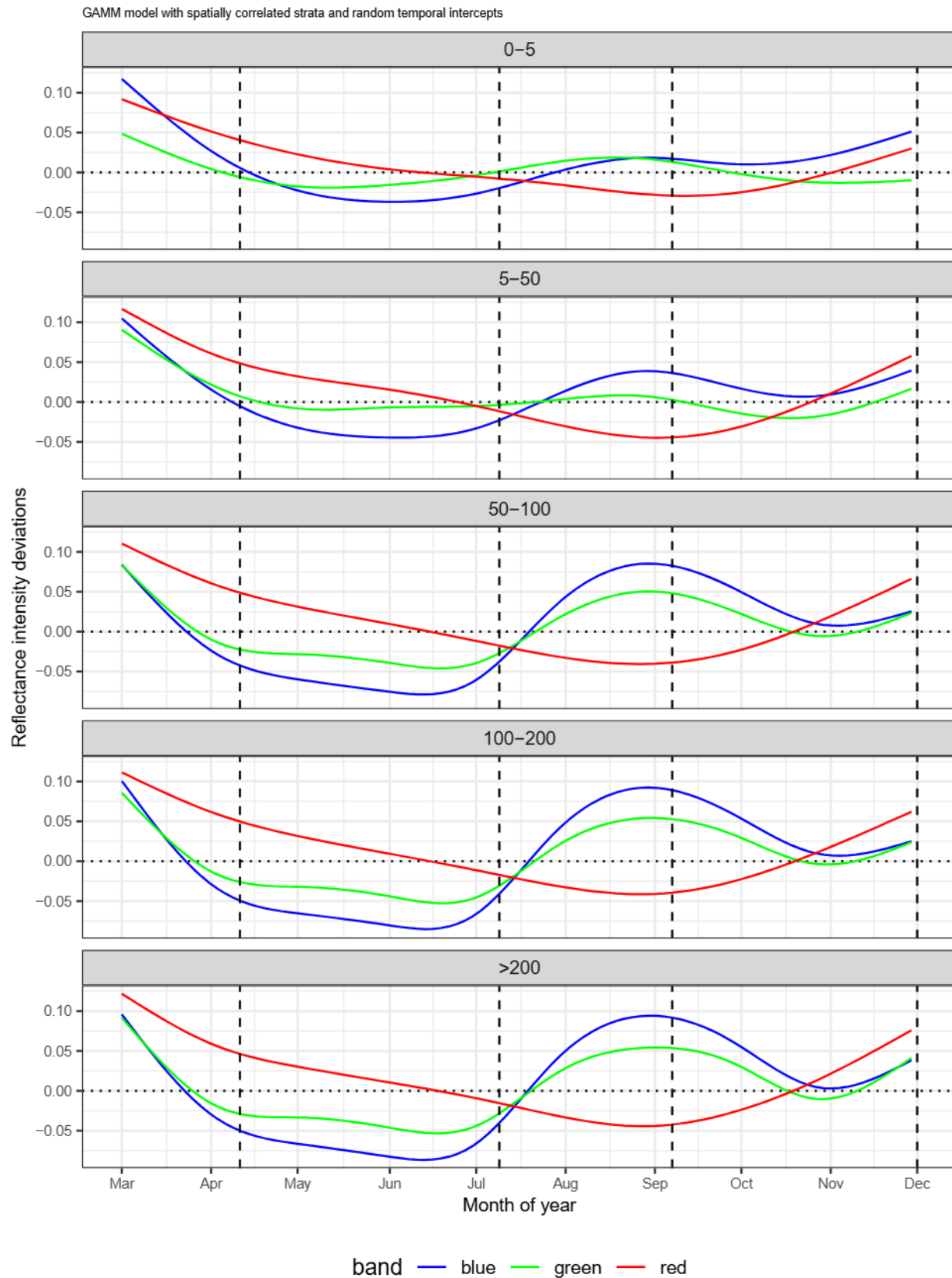


Figure 10. Seasonal variation of Sentinel 2 reflectances by color band and depth intervals from Torch Lake in Antrim County, Michigan

Preprint. Not peer reviewed.



(a) Figure based on previous analysis by D.J. Holtschlag, 2024, <https://eartharxiv.org/repository/view/7653>

Figure 11. Seasonal variation of Landsat reflectances by color band and depth intervals from Torch Lake in Antrim County, Michigan

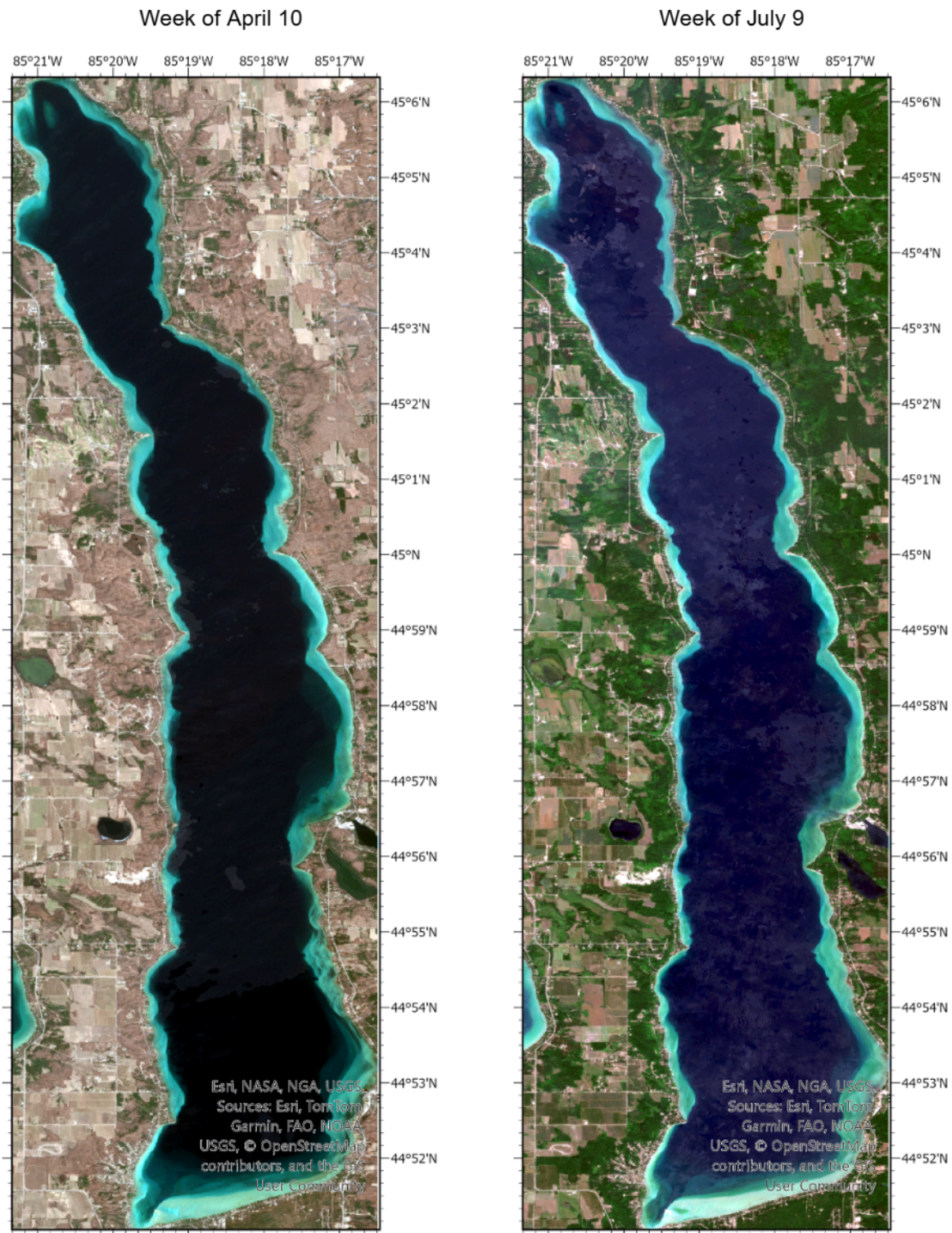


Figure 12. Composite satellite images of Torch Lake showing seasonal reflectances for the weeks of April 10 and July 9 during 2019-2025 in Antrim County, Michigan

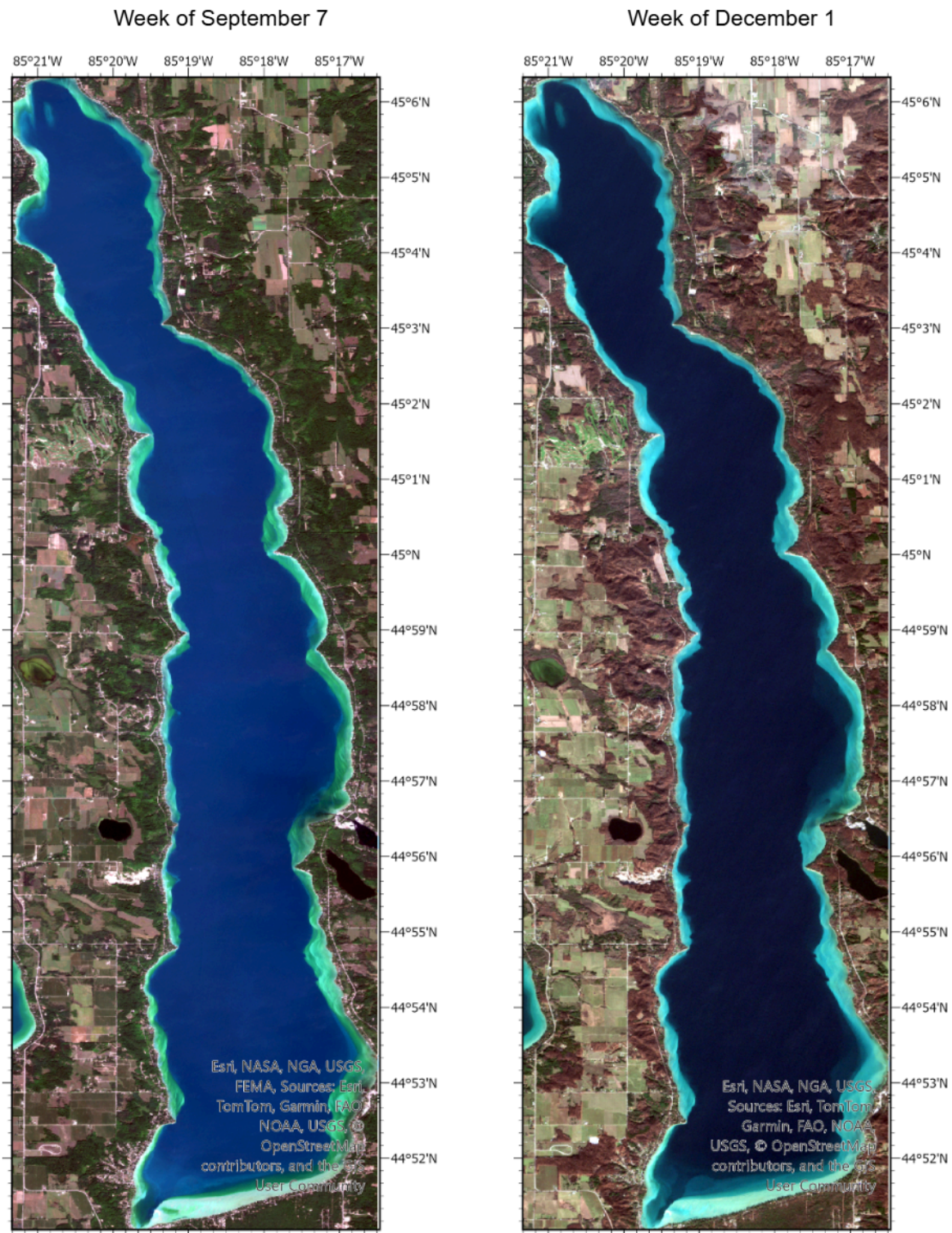


Figure 13. Composite satellite images of Torch Lake showing seasonal reflectances for the weeks of September 7 and December 1 during 2019-2025 in Antrim County, Michigan

## Random Effects and Error Correlation

A random intercept model is a special case of a random effects model in which an intercept term describes the random component. More generally, a random effects model might include a random intercept, serving as a starting point, as well as a random slope component, which would allow the rate of change in the random component to change with a selected variable. In this analysis, random intercept models were considered sufficient to describe the random effects without the addition of a random slope.

Random intercept models were applied individually to both spatial and temporal components. Strata was used to define the spatial component, whereas day of the satellite image defined the temporal component. In the case where individual strata commonly had different average responses, a spatial intercept component may have been dominant. When the random intercept effects were assessed by strata, error correlation effects were assessed by the time between images.

Alternatively, when random intercept effects were assessed based on the date of an image and different dates had different average responses, a temporal intercept component may have been dominant. When the random intercepts were dates, the spatial error correlation was assessed based on the separation distances between strata. The BIC statistic was used to assess the preferred model.

## GAMM ID3: Spatial Random Intercepts and Temporal Error Correlation

The spatial random intercepts  $b_{0i}$  discussed in this section were computed by use of GAMM ID3 based on  $n = 287$  (daily) measurements for each of the 60 strata in the blue, green, and red bands. Outlying random intercepts are of interest because they identify strata that have anomalous departures from other random intercepts given the fixed effects described by the model. These departures may help identify strata that have surface reflectances that have different or more pronounced effects of physical, chemical, or biological processes than those generally occurring in Torch Lake. The occurrence of outliers in multiple reflectance bands within the same strata may provide additional insight into the nature of these anomalies.

Identifying outliers can be problematic because the properties of the distribution of random intercepts is not precisely known. This analysis assumes that the residuals are approximately normally distributed with mean zero. To provide a more robust indicator of variance than the standard deviation, however, the Median Absolute Deviation (MAD) is used here to identify outliers. Steps used to compute the MAD and associated modified z-scores are provided in the following.

### MAD-Based Outlier Detection:

- |  |  |
|--|--|
| For random intercepts ( $b_{0i}$ )     | $\epsilon = \{\epsilon_1, \epsilon_2, \dots, \epsilon_n\}$                         |
| Step 1: Calculate the median:          | $\tilde{\epsilon} = \text{median}(\epsilon)$                                       |
| Step 2: Calculate the MAD:             | $\text{MAD}(\epsilon) = \text{median}( \epsilon - \tilde{\epsilon} )$              |
| Step 3: Calculate modified z-scores:   | $z_i^* = 0.6745 \times \frac{\epsilon_i - \tilde{\epsilon}}{\text{MAD}(\epsilon)}$ |
| where $0.6745 \approx \Phi^{-1}(0.75)$ | (the 75th percentile of the standard normal distribution)                          |
| Step 4: Outliers were identified for   | $ z_i^*  > 4.0$ .  |

Figure 14 shows modified z-scores by strata and color band. (Numerical values are shown in

appendix table 2 with outliers underlined). Note that strata NNE1 and NCE1 are negative outliers for all color bands, and strata SSW1 are positive for all bands. Strata SSW1 is at the outlet of Torch Lake, which forms Torch River that is monitored by streamgage 04127570. Strata NSW2 and SNE2 are negative and NCE2 and NSE2 are positive for the blue and green bands. Note that the SNE2 strata receives flow from Clam Lake Outlet, which is monitored at streamgage 041275685. NCW2 and SCE2 are positive for the green band, and NSE1 is positive for the red band.

It is noteworthy that all identified outlier strata are in the shallow (<50 ft) water-depth intervals (indicated by the fourth character in the strata identifier as 1 or 2). although this may be coincidental, it seems more likely that the water-depth intervals do not adequately define the shallow water-depth characteristics affecting surface reflectance from these strata. Improved bathymetry data in the shallow water-level areas would help resolve this concern and enable the development of a continuous function describing the relation between water-depths and surface reflectances. NASA's ICESat-2 ATL13 coverage may aid future studies in resolving this uncertainty by providing tracks of water-level and bathymetry data in shallow areas of inland lakes to supplement existing bathymetry data collection methods.

Synoptic field sampling from strata characterized as outliers for physical, chemical, and biological components that affect surface reflectance may also help better understand underlying processes in Torch Lake.

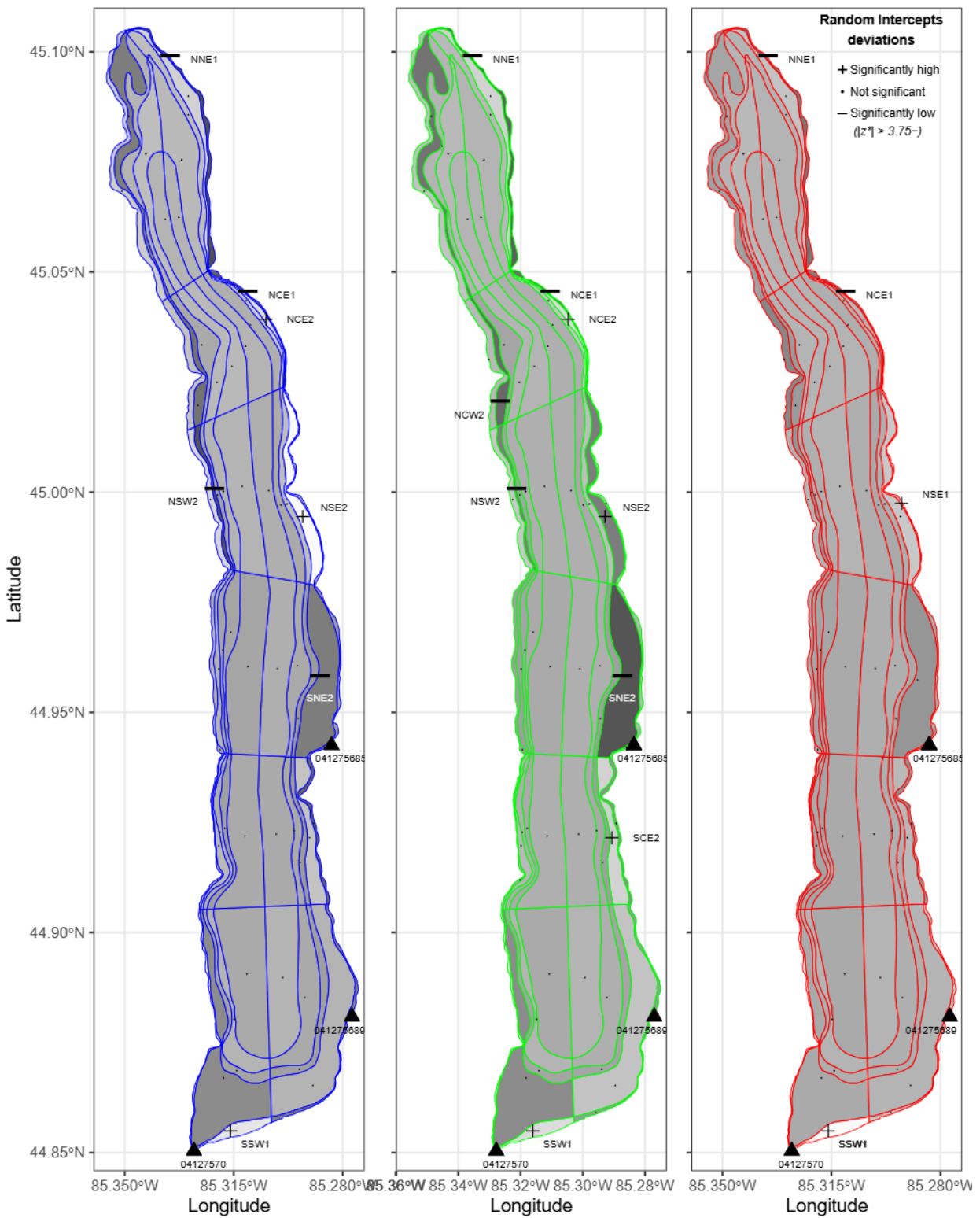


Figure 14. Torch Lake with strata fill colors based on GAMM ID3 spatial random intercepts in Antrim County, Michigan

A common assumption underlying many statistical models is that errors (residuals) are normally distributed, independent (uncorrelated), and identically distributed, which is true for GAMMs as well (eqn. 1). When errors are (positively) correlated, the effective number of measurements is less than the sample size, thereby making tests of model significance unreliable and model selection problematic.

In this modelling framework, model errors can be correlated in time or space. The temporal correlation in the GAMM ID3 was estimated as a model parameter and shown in figure 15. The correlation length is shortest for the red band, which is essentially zero after more than two days of separation; blue and green bands had little correlation after five days of separation.

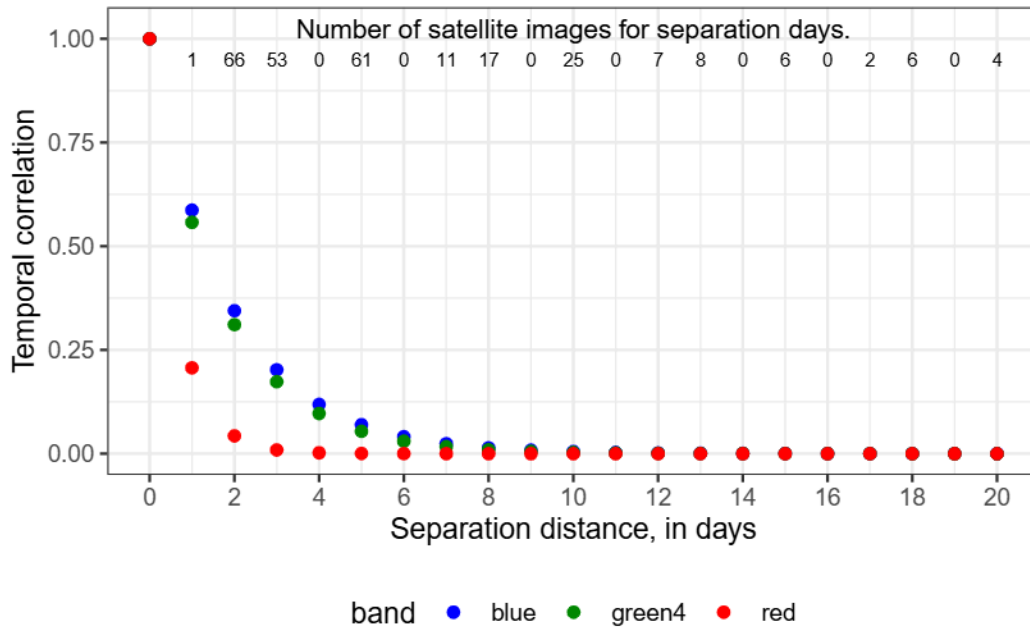


Figure 15. Relation between error correlation and temporal separation distances between selected images on Torch Lake in Antrim County, Michigan

#### GAMM ID4: Temporal Random Intercepts and Spatial Error Correlation

Figure 16 shows the temporal random intercepts that represents the systematic bias on each satellite image indexed by the date of measurement in the model's estimate over all 60 strata. So, the measured (and transformed) reflectance is decomposed into a prediction based on fixed and smooth plus temporal random intercept(deltaDays) plus the residual error. The complex spatial correlation structure prevented individual standard error calculation. Therefore, The standard error of the individual temporal random components was approximated as the standard deviation of the intercept components within each band.

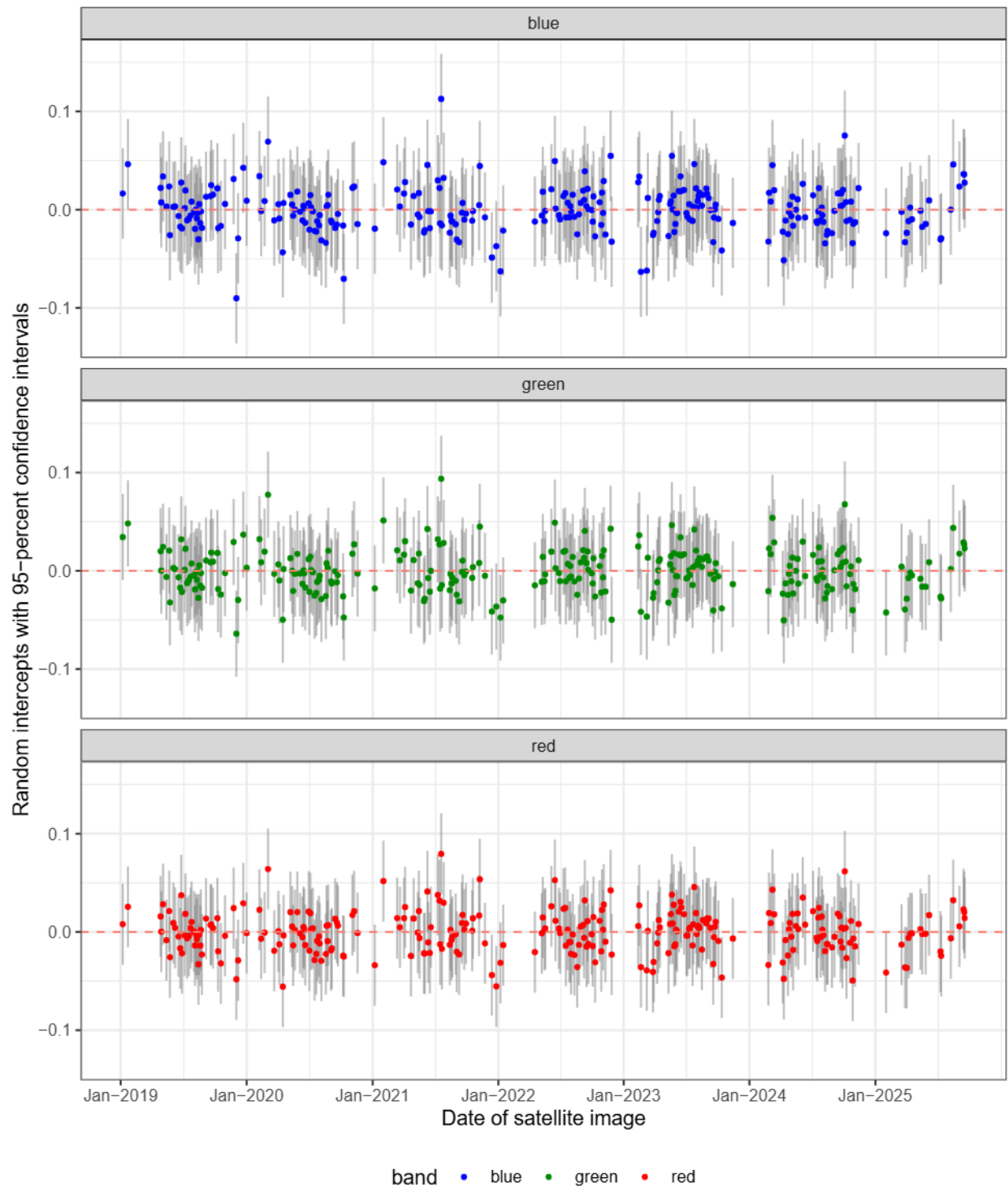


Figure 16. Random temporal intercepts by date of Sentinel 2 image of Torch Lake in Antrim County, Michigan

Figure 17 shows the exponential decline in spatial correlation with distance between strata centroids computed by use of GAMM ID4. The most rapid decline occurs in the green band, followed slower rates of decrease in the blue and red bands, respectively. Most of the spatial correlation occurred at separation distances of less than 3 kilometers. Note that the temporal correlations had the shortest range in the red band, with longer correlation ranges in both the blue and green bands.

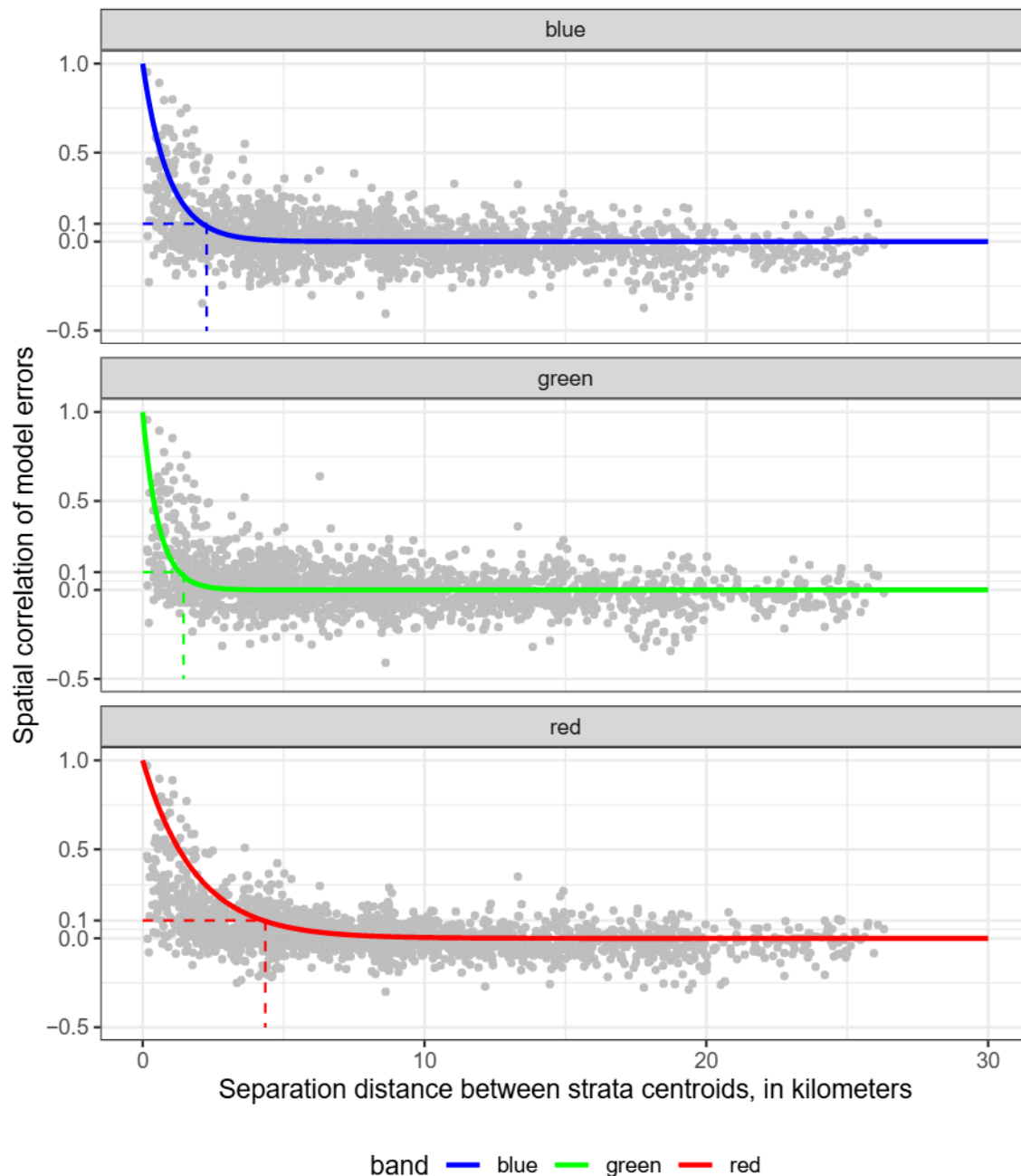


Figure 17. Spatial correlation of GAMM ID4 errors as a function of strata separation distances

## Conclusions

Surface reflections of blue, green, and red bands of visible light from Torch Lake were analyzed based on ESAs Sentinel 2 satellite images. The 287 images analyzed were surface reflectances obtained from 2019 to 2025. Each image captured median reflectances from 10-m square pixels in 60 variously sized strata that spanned the surface area of Torch Lake. The strata partitioned the lake into five water-depth intervals, six north-south extents, and two east-west extents. Strata better enabled the analysis of benthic reflections from shallow areas and water-column reflections in deeper areas.

Four statistical models were developed to describe the spatial and temporal variation in surface reflectances from Torch Lake. All four models included the same fixed and smooth effects. The first model, GAM ID1, a generalized additive model was applied which does not explicitly account for random effects or error correlation. The second model GAMM ID2 accounted for random effects within the smooth components. GAMM ID3 also accounted for spatial random intercepts in strata and temporal error correlation. GAMM ID4 accounted for temporal random effects (as intercepts), which were associated with uncorrected variations in atmospheric effects, and spatial autocorrelation associated with redundancies in sampling closely spaced strata. The GAMM ID4 was selected because it had substantially lower root-mean-square error and Bayesian Information Criteria (BIC) statistics for all bands.

In GAMM ID3, outliers identified in random intercepts of strata occurred exclusively in shallow water-depth strata, including at the outlet of Clam River, which is a source of nutrients and dissolved and suspended materials to Torch Lake. Interpreting outliers in random intercepts of shallow areas, however, is problematic because of the uncertainties in shallow-water depths provided by coarse bathymetry contours. A digital elevation model (DEM) of shallow-water depths may help to better distinguish effects of water depths from changes in benthic characteristics. Bathymetry data from NASA's ICESat-2 satellite may aid the development of a high-quality DEM. Such a DEM may help to define a continuous relation between water depth and reflectance, and aid the identification of spatial anomalies in water quality to provide a better focus for field water-quality sampling.

Sentinel 2 data is successfully processed to reduce the random effects associated with daily changes in atmospheric distortion. Few applications of satellite data analysis would be successful without these skillful corrections. The GAMM ID4 shows, however, that much of the residual temporal error can be accounted for by application of generalized additive mixed models with temporal random intercepts. In addition, GAMM ID4 helps account for spatial error correlation, which reduces the effective number of observations. Without this reduction, the model statistics would be biased to overstate the significance of model parameters. Thus, generalized additive mixed models provide fixed, smooth, and random effects to better characterize surface reflectances from satellite imagery and quantify error correlation to reduce effects of sampling redundancy.

## References Cited

- Allaire, JJ, and Christophe Dervieux. 2024. Quarto: R Interface to 'Quarto' Markdown Publishing System. <https://doi.org/10.32614/CRAN.package.quarto>.
- European Space Agency. 2025. "Applications: Sentinel-2 Color Vision for Copernicus." [https://www.esa.int/Applications/Observing\\_the\\_Earth/Copernicus/Sentinel-2](https://www.esa.int/Applications/Observing_the_Earth/Copernicus/Sentinel-2); European Space Agency. 2025.
- Holtschlag, J., David. 2024. "A Preliminary Analysis of Landsat Surface-Reflectance Data from Torch Lake in Antrim County, Michigan, USA from 1984 to 2023." <https://eartharxiv.org/repository/view/7653/>; Posted as a preprint on Earth ArXiv. <https://doi.org/10.31223/X5CH81>.
- Jasinski, M. F., J. D. Stoll, D. Hancock, and the ICESat-2 Science Team. 2023. ATLAS/ICESat-2 L3A Along Track Inland Surface Water Data, Version 6. NASA National Snow; Ice Data Center Distributed Active Archive Center, Boulder, Colorado USA. <https://doi.org/https://doi.org/10.5067/ATLAS/ATL13.006>.
- Levesque, V. A., and K. A. Oberg. 2012. "Computing Discharge Using the Index Velocity Method." Edited by U. S. Geological Survey. Techniques and Methods. Reston, VA. <https://doi.org/10.3133/tm3A23>.
- R Core Team. 2025a. R: A Language and Environment for Statistical Computing. Vienna, Austria: R Foundation for Statistical Computing. <https://www.R-project.org/>.
- . 2025b. R: A Language and Environment for Statistical Computing. Vienna, Austria: R Foundation for Statistical Computing. <https://www.R-project.org/>.
- Stevenson, R. Jan. 2016. "2016 Study of Golden Brown Algae on the Bottom of Torch Lake, Lake Bellaire, and Clam Lake." Available at: <https://www.3lakes.com/wp-content/uploads/2015/02/2016-RJS-Report-TLA-GBA.pdf>, 44p.; Dr. Stevenson is a Professor Emeritus in the Department of Integrative Biology; Center for Water Sciences at Michigan State University.
- Three Lakes Association. 2004. "Cooperative Lakes Monitoring Program." Available at: <https://www.3lakes.com/projects/cooperative-lakes-monitoring-program/>; Three Lakes Association, Accessed: April 25, 2025.
- Tip of the Mitt Watershed Council. 2024. "Torch Lake." Available at: <https://watershedcouncil.org/waterbody/torch-lake/>; Tip of the Mitt Watershed Council. Accessed: April 25, 2025.
- U.S. Geological Survey. 2003a. "USGS 445850085180401: North Basin Torch Lake near Creswell, MI." Available at: <https://waterdata.usgs.gov/monitoring-location/450140085185601/>; National Water Information System, Accessed: April 25, 2025.
- . 2003b. "USGS 445850085180401: South Basin Torch Lake near Creswell, MI." Available at: <https://waterdata.usgs.gov/monitoring-location/445850085180401/>; National Water Information System, Accessed: April 25, 2025.
- Wickham, Hadley. 2016. Ggplot2: Elegant Graphics for Data Analysis. Springer-Verlag New York. <https://ggplot2.tidyverse.org>.
- Wood, Simon N. 2017. Generalized Additive Models: An Introduction with r. 2nd ed. Chapman; Hall/CRC. <https://doi.org/10.1201/9781315370279>.

## Appendices

### Appendix 1. Acknowledgements

The author gratefully acknowledges the contributions of Alphabet Corporation in providing free access to the Google Earth Engine (GEE) environment (<https://earthengine.google.com/>), which was used to access and process Sentinel 2 data. The work would not have been possible without GEE. The author also is grateful for access to Anthropic's artificial intelligence Large Language Model Claude (<https://claude.ai/new>), which wrote much of the javascript code used within GEE to access and summarize satellite data, and numerous coding tasks in the R scientific programming and computing environment. Claude is especially adept in the esoteric knowledge of the syntax for the LaTeX preamble packages that are in the quarto script used to generate the manuscript. These packages were essential for formatting the document to print as a technical report. Finally, I would be amiss not to recognize the many assists that Claude provides to generating figures in ESRI's ArcGIS Pro.

## Appendix 2. Horizontal strata partitioning of Torch Lake with GAMM ID3 spatial random intercepts.

Table 1. Strata naming, water-depths, area, and locational information for Torch Lake in Antrim County, Michigan

Strata		Water Depth	Area		MI GeoRef (miles)		Spatial Random Intercept		
Order	Name	Interval (ft)	(in pixels)	(sq. miles)	Northing	Easting	Blue	Green	Red
1	NNW1	0-5	9037	0.3489179	311.9664	342.3269	0.014154	0.015684	-0.008717
2	NNW2	5-50	14148	0.5462525	313.1348	342.4372	-0.014354	-0.032151	-0.005540
3	NNW3	50-100	12396	0.4786131	312.6713	342.6095	0.002543	0.001767	0.004413
4	NNW4	100-200	16613	0.6414139	312.5577	342.7115	0.006545	0.007071	0.006411
5	NNW5	200-300	13090	0.5053896	311.5264	343.0215	0.002381	0.002363	0.002582
6	NNE5	200-300	10021	0.3869132	311.5581	343.2316	0.002571	0.002256	0.002624
7	NNE4	100-200	25631	0.9896314	312.4603	343.2707	0.004964	0.004977	0.004257
8	NNE3	50-100	9824	0.3793229	313.1448	343.3812	0.006532	0.008105	0.005019
9	NNE2	5-50	9271	0.3579432	313.4390	343.3810	0.016797	0.032890	0.016705
10	<u>NNE1</u>	0-5	4466	0.1724462	313.5733	343.4527	<u>-0.028711</u>	<u>-0.043395</u>	<u>-0.028553</u>
11	NCW1	0-5	5960	0.2301087	309.3316	343.3728	0.008907	0.008820	-0.020448
12	<u>NCW2</u>	5-50	5238	0.2022470	308.6075	343.5512	-0.017760	<u>-0.037805</u>	-0.009809
13	NCW3	50-100	8311	0.3208891	309.5608	343.6088	-0.002017	-0.004977	0.001436
14	NCW4	100-200	10425	0.4025137	308.9477	343.8462	0.003365	0.002412	0.002984
15	NCW5	200-300	14982	0.5784403	309.2243	344.0898	0.003689	0.003366	0.004153
16	NCE5	200-300	14715	0.5681323	309.5481	344.3005	0.000903	0.000330	0.001740
17	NCE4	100-200	9672	0.3734400	309.8821	344.3721	0.000196	-0.000113	0.000365
18	NCE3	50-100	2869	0.1107918	310.2581	344.3030	0.014661	0.022381	0.004648
19	<u>NCE2</u>	5-50	2294	0.0885579	309.9678	344.6209	<u>0.024853</u>	<u>0.041118</u>	0.009562
20	<u>NCE1</u>	0-5	1328	0.0512889	310.3492	344.3294	<u>-0.022661</u>	<u>-0.034416</u>	<u>-0.024520</u>
21	NSW1	0-5	5190	0.2003914	307.1377	343.7660	0.020384	0.021134	0.004258
22	<u>NSW2</u>	5-50	3066	0.1183856	306.4409	343.9847	<u>-0.027478</u>	<u>-0.051163</u>	-0.013866
23	NSW3	50-100	3453	0.1333233	307.2104	343.8795	-0.002860	-0.004917	-0.001762
24	NSW4	100-200	9193	0.3549581	307.2659	343.9715	0.000709	0.000312	-0.000081
25	NSW5	200-300	29830	1.1517578	307.3479	344.2642	0.000725	0.000208	0.000619
26	NSE5	200-300	25961	1.0023677	307.2869	344.6823	-0.001118	-0.001576	-0.000274
27	NSE4	100-200	11161	0.4309445	307.0934	344.8664	-0.002597	-0.003397	-0.002736
28	NSE3	50-100	6826	0.2635498	306.8564	345.1012	0.006526	0.010935	0.000405
29	<u>NSE2</u>	5-50	11078	0.4277290	306.8985	345.2152	<u>0.038863</u>	<u>0.069191</u>	0.021188
30	<u>NSE1</u>	0-5	1504	0.0580881	307.2260	345.0687	0.015106	0.022962	<u>0.023377</u>

(continued)

Order	Name	Interval (ft)	(in pixels)	(sq. miles)	Northing	Easting	Blue	Green	Red
31	SNW1	0-5	3675	0.1419017	303.2350	343.9332	0.002824	-0.007708	-0.003739
32	SNW2	5-50	4994	0.1928043	304.4839	343.9219	0.001362	-0.009178	-0.005627
33	SNW3	50-100	4903	0.1893232	304.7792	343.9807	-0.003649	-0.004744	-0.005714
34	SNW4	100-200	8509	0.3285251	305.0626	344.1056	-0.003636	-0.004062	-0.005329
35	SNW5	200-300	36653	1.4151760	304.5238	344.3780	-0.002723	-0.002949	-0.003997
36	SNE5	200-300	30933	1.1943241	304.4989	344.8467	-0.001213	-0.000429	-0.001513
37	SNE4	100-200	11458	0.4424031	304.5453	345.1581	-0.001334	-0.000769	0.000082
38	SNE3	50-100	5943	0.2294607	303.7266	345.1784	-0.006269	-0.008899	-0.002167
39	<u>SNE2</u>	5-50	27828	1.0744433	304.3232	345.5121	<u>-0.031171</u>	<u>-0.049142</u>	-0.013562
40	SNE1	0-5	2632	0.1016310	303.2677	345.5874	-0.004811	0.005567	-0.003230
41	SCW1	0-5	1256	0.0485042	301.1718	343.9255	0.001563	-0.001701	-0.011776
42	SCW2	5-50	3923	0.1514494	301.7128	343.9436	0.005564	0.005480	-0.006120
43	SCW3	50-100	4519	0.1744642	301.9238	343.9601	-0.000616	0.000402	-0.003215
44	SCW4	100-200	5642	0.2178525	301.9876	344.0370	-0.004263	-0.003328	-0.005716
45	SCW5	200-300	31838	1.2292845	301.8684	344.3521	-0.002313	-0.002122	-0.003085
46	SCE5	200-300	28008	1.0813984	301.9024	344.8474	-0.001852	-0.001556	-0.001818
47	SCE4	100-200	6853	0.2645807	301.9588	345.1318	-0.002635	-0.002740	-0.001813
48	SCE3	50-100	4700	0.1814872	301.4765	345.2275	-0.006592	-0.008135	-0.001598
49	<u>SCE2</u>	5-50	10195	0.3936351	301.8512	345.3725	0.010877	<u>0.034190</u>	0.008433
50	SCE1	0-5	2769	0.1069176	302.0770	345.4381	-0.022326	-0.017338	-0.016152
51	<u>SSW1</u>	0-5	6354	0.2453110	297.2442	344.1664	<u>0.029100</u>	<u>0.040665</u>	<u>0.067154</u>
52	SSW2	5-50	34569	1.3347267	298.0735	344.0510	-0.010518	-0.018867	-0.004487
53	SSW3	50-100	6704	0.2588287	298.0768	344.5162	-0.003333	-0.004844	0.000332
54	SSW4	100-200	10283	0.3970202	298.9946	344.2123	0.000466	0.001262	0.001194
55	SSW5	200-300	37113	1.4329481	299.7049	344.4047	-0.002534	-0.002372	-0.002733
56	SSE5	200-300	29381	1.1344012	299.6547	344.9676	0.001485	0.002481	0.001701
57	SSE4	100-200	19691	0.7602843	299.3437	345.3174	-0.001779	-0.001623	0.000383
58	SSE3	50-100	9138	0.3528214	298.2193	345.2391	-0.004925	-0.007074	-0.001797
59	SSE2	5-50	35854	1.3843439	297.9662	345.4520	0.002963	0.015436	0.003122
60	SSE1	0-5	3286	0.1268663	297.5387	345.1495	-0.013530	-0.010273	0.022346

### Appendix 3. JavaScript used in Google Earth Engine to access imagery by Anthropic's Claude, September 2025

```
// TL_Sentinel/S2_HARMONIZED/TLS2s60_scale20m_2025Jan02a

// Define the bounding box for Torch Lake
var torchLakeBbox = ee.Geometry.Rectangle([-85.40, 44.825, -85.25, 45.125]);

// Harmonized Sentinel-2 Level 2A collection
var s2 = ee.ImageCollection('COPERNICUS/S2_SR_HARMONIZED');
// Cloud Score+ image collection
var csPlus = ee.ImageCollection('GOOGLE/CLOUD_SCORE_PLUS/V1/S2_HARMONIZED');

var QA_BAND = 'cs_cdf';
var CLEAR_THRESHOLD = 0.60;

// Function to calculate GBA-related indices
function addGBAIndices(image) {
  // Basic pigment index (Green-Blue ratio)
  var pigmentIndex = image.expression(
    '(GREEN - BLUE) / (GREEN + BLUE)', {
      'GREEN': image.select('B3'),
      'BLUE': image.select('B2')
    }).rename('pigment_index');

  // Red edge position index
  var redEdgeIndex = image.expression(
    '(RE1 - RED) / (RE1 + RED)', {
      'RE1': image.select('B5'),
      'RED': image.select('B4')
    }).rename('red_edge_index');

  // Enhanced vegetation index (modified for aquatic environment)
  var eviAquatic = image.expression(
    '2.5 * (NIR - RED) / (NIR + 6 * RED - 7.5 * BLUE + 1)', {
      'NIR': image.select('B8'),
      'RED': image.select('B4'),
      'BLUE': image.select('B2')
    }).rename('evi_aquatic');

  // Green ratio
  var greenRatio = image.expression(
    'GREEN / (BLUE + RED + RE1)', {
      'GREEN': image.select('B3'),
      'BLUE': image.select('B2'),
      'RED': image.select('B4'),

```

```

    'RE1': image.select('B5')
  }).rename('green_ratio');

return image
  .addBands(pigmentIndex)
  .addBands(redEdgeIndex)
  .addBands(eviAquatic)
  .addBands(greenRatio);
}

// Function to compute statistics and mask counts for each polygon
function computeStatsAndMasks(image) {
  // Set consistent scale across all calculations
  var ANALYSIS_SCALE = 10; // Using 20m scale to match SCL band

  var cloudScore = image.select(QA_BAND).reduceRegion({
    reducer: ee.Reducer.mean(),
    geometry: roi.geometry(),
    scale: ANALYSIS_SCALE,
    maxPixels: 1e9
  }).get(QA_BAND);

  // Scene Classification Layer masks
  var scl = image.select('SCL');
  var waterMask = scl.eq(6); // Water class in SCL

  // Create a valid pixel mask (1 where we have valid data, 0 otherwise)
  var validPixelMask = scl.gte(1).and(scl.lte(11));

  var selectedImage = image.select([
    'B2', 'B3', 'B4', 'B5', 'B6',
    'pigment_index', 'red_edge_index', 'evi_aquatic', 'green_ratio'
  ]);

  var reduced = roi.map(function(feature) {
    // Get the geometry
    var geom = feature.geometry();

    // Calculate total valid pixels using SCL band
    var totalPixels = validPixelMask.reduceRegion({
      reducer: ee.Reducer.sum(),
      geometry: geom,
      scale: ANALYSIS_SCALE,
      maxPixels: 1e9
    }).get('SCL');

    // Calculate geometry pixels

```

```

var geometryPixels = ee.Image.constant(1).updateMask(validPixelMask).reduceRegion({
  reducer: ee.Reducer.count(),
  geometry: geom,
  scale: ANALYSIS_SCALE,
  maxPixels: 1e9
}).get('constant');

// Calculate individual SCL class masks
var sclCounts = ee.Dictionary({
  'saturated_pixels': scl.eq(1),
  'dark_features_pixels': scl.eq(2),
  'shadow_pixels': scl.eq(3),
  'vegetation_pixels': scl.eq(4),
  'bare_soil_pixels': scl.eq(5),
  'water_pixels': scl.eq(6),
  'unclassified_pixels': scl.eq(7),
  'cloud_medium_prob_pixels': scl.eq(8),
  'cloud_high_prob_pixels': scl.eq(9),
  'thin_cirrus_pixels': scl.eq(10),
  'snow_ice_pixels': scl.eq(11)
}).map(function(key, mask) {
  return ee.Image(mask).reduceRegion({
    reducer: ee.Reducer.sum(),
    geometry: geom,
    scale: ANALYSIS_SCALE,
    maxPixels: 1e9
  }).get('SCL');
});

// Calculate statistics for selected bands
var statistics = selectedImage.reduceRegion({
  reducer: ee.Reducer.mean().combine({
    reducer2: ee.Reducer.median(),
    sharedInputs: true
  }).combine({
    reducer2: ee.Reducer.percentile([0, 2, 5, 10, 25, 50, 75, 90, 95, 98, 100]),
    sharedInputs: true
  }).combine({
    reducer2: ee.Reducer.count(),
    sharedInputs: true
  }).combine({
    reducer2: ee.Reducer.stdDev(),
    sharedInputs: true
  }),
  geometry: geom,
  scale: ANALYSIS_SCALE, // Using consistent scale
  maxPixels: 1e9

```

```

    });

// Add pixel count validation
var pixelCountCheck = ee.Dictionary({
  'geometry_pixels': geometryPixels,
  'total_pixels': totalPixels,
  'pixel_count_difference': ee.Number(geometryPixels).subtract(totalPixels),
  'pixel_count_match': ee.Number(geometryPixels).eq(totalPixels)
});

// Calculate percentages using total valid pixels
// First, collect keys and values separately
var percentageKeys = sclCounts.keys().map(function(key) {
  return ee.String(key).cat('_percentage');
});
var percentageValues = sclCounts.values().map(function(value) {
  return ee.Number(value).divide(totalPixels).multiply(100);
});

// Create dictionary from the keys and values
var maskPercentages = ee.Dictionary.fromLists(percentageKeys, percentageValues);

return feature
  .set(statistics)
  .set(sclCounts)
  .set(maskPercentages)
  .set(pixelCountCheck)
  .set('DATATAKE_IDENTIFIER', image.get('DATATAKE_IDENTIFIER'))
  .set('PRODUCT_ID', image.get('PRODUCT_ID'))
  .set('MGRS_TILE', image.get('MGRS_TILE'))
  .set('ORBIT_NUMBER', image.get('ORBIT_NUMBER'))
  .set('MEAN_SOLAR_AZIMUTH_ANGLE', image.get('MEAN_SOLAR_AZIMUTH_ANGLE'))
  .set('MEAN_SOLAR_ZENITH_ANGLE', image.get('MEAN_SOLAR_ZENITH_ANGLE'))
  .set('CLOUDY_PIXEL_PERCENTAGE', image.get('CLOUDY_PIXEL_PERCENTAGE'))
  .set('cloud_score', cloudScore)
  .set('system:time_start', image.get('system:time_start'))
  .set('DATE', ee.Date(image.get('system:time_start')).format('yyyy-MM-dd'))
  .set('year', ee.Date(image.get('system:time_start')).get('year'))
  .set('month', ee.Date(image.get('system:time_start')).get('month'))
  .set('doy', ee.Date(image.get('system:time_start')).getRelative('day', 'year'));
});

return reduced;
}

var s2_base = s2.filterBounds(torchLakeBbox)

```

```

        .filter(ee.Filter.eq('MGRS_TILE', '16TFQ'));

// Get and print first and last dates in a readable format
var firstImage = ee.Date(s2_base.first().get('system:time_start'));
var lastImage = ee.Date(s2_base.sort('system:time_start', false).first().get('system:time_start'));

print('First available date:', firstImage.format('YYYY-MM-dd').getInfo());
print('Last available date:', lastImage.format('YYYY-MM-dd').getInfo());

// Function to filter image collection by specific dates
function filterImagesByDates(collection, dateList) {
  // Convert date strings to ee.Date objects and create filters
  var dateFilters = dateList.map(function(date) {
    var eeDate = ee.Date(date);
    return ee.Filter.date(eeDate, eeDate.advance(1, 'day'));
  });

  // Create a single OR filter from all date filters
  var combinedFilter = ee.Filter.or.apply(null, dateFilters);

  // Apply the filter to the collection
  return collection.filter(combinedFilter);
}

// print('s2 is: ', s2)

print('s2 collection info:', {
  'collection type': s2.get('system:id'),
  'first image date': ee.Date(s2.first().get('system:time_start')).format('YYYY-MM-dd'),
  'bands': ee.Image(s2.first()).bandNames()
});

var dateList = [
  '2018-12-14', '2018-12-29', '2019-01-06', '2019-01-21', '2019-03-29', '2019-04-03',
  '2019-04-26', '2019-04-28', '2019-05-03', '2019-05-13', '2019-05-21', '2019-05-23',
  '2019-05-26', '2019-06-02', '2019-06-07', '2019-06-17', '2019-06-22', '2019-06-25',
  '2019-06-27', '2019-07-05', '2019-07-07', '2019-07-10', '2019-07-12', '2019-07-17',
  '2019-07-22', '2019-07-25', '2019-07-30', '2019-08-01', '2019-08-04', '2019-08-06',
  '2019-08-09', '2019-08-11', '2019-08-14', '2019-08-16', '2019-08-19', '2019-08-21',
  '2019-08-24', '2019-09-03', '2019-09-05', '2019-09-18', '2019-09-20', '2019-09-25',
  '2019-10-08', '2019-10-10', '2019-10-18', '2019-10-30', '2019-11-24', '2019-12-02',
  '2019-12-07', '2019-12-22', '2020-01-01', '2020-02-07', '2020-02-10', '2020-02-12',
  '2020-02-17', '2020-02-22', '2020-03-03', '2020-03-21', '2020-04-02', '2020-04-05',
  '2020-04-15', '2020-04-17', '2020-05-07', '2020-05-12', '2020-05-15', '2020-05-20',
  '2020-05-27', '2020-06-04', '2020-06-11', '2020-06-14', '2020-06-16', '2020-06-19',
  '2020-06-26', '2020-06-29', '2020-07-01', '2020-07-04', '2020-07-06', '2020-07-11',

```

```

'2020-07-16', '2020-07-19', '2020-07-21', '2020-07-24', '2020-07-29', '2020-07-31',
'2020-08-05', '2020-08-15', '2020-08-18', '2020-08-20', '2020-08-23', '2020-08-25',
'2020-09-02', '2020-09-04', '2020-09-07', '2020-09-14', '2020-09-17', '2020-09-19',
'2020-09-22', '2020-09-24', '2020-10-07', '2020-10-09', '2020-11-03', '2020-11-08',
'2020-11-18', '2021-01-07', '2021-01-25', '2021-01-30', '2021-02-01', '2021-02-26',
'2021-03-03', '2021-03-06', '2021-03-08', '2021-03-13', '2021-03-21', '2021-04-02',
'2021-04-05', '2021-04-10', '2021-04-17', '2021-04-22', '2021-04-30', '2021-05-12',
'2021-05-15', '2021-05-17', '2021-05-22', '2021-05-30', '2021-06-01', '2021-06-09',
'2021-06-11', '2021-06-16', '2021-06-19', '2021-07-01', '2021-07-09', '2021-07-14',
'2021-07-16', '2021-07-19', '2021-07-21', '2021-07-26', '2021-08-03', '2021-08-13',
'2021-08-15', '2021-08-18', '2021-08-20', '2021-08-25', '2021-08-30', '2021-09-02',
'2021-09-09', '2021-09-14', '2021-09-17', '2021-09-19', '2021-09-24', '2021-09-29',
'2021-10-07', '2021-10-17', '2021-10-19', '2021-11-06', '2021-11-08', '2021-11-23',
'2021-11-28', '2021-12-13', '2021-12-26', '2022-01-07', '2022-01-15', '2022-01-30',
'2022-04-10', '2022-04-17', '2022-05-07', '2022-05-10', '2022-05-15', '2022-05-17',
'2022-06-04', '2022-06-09', '2022-06-14', '2022-06-16', '2022-06-26', '2022-06-29',
'2022-07-09', '2022-07-14', '2022-07-16', '2022-07-21', '2022-07-26', '2022-07-29',
'2022-07-31', '2022-08-05', '2022-08-10', '2022-08-18', '2022-08-23', '2022-08-28',
'2022-09-04', '2022-09-07', '2022-09-09', '2022-09-14', '2022-09-17', '2022-09-19',
'2022-09-22', '2022-09-29', '2022-10-02', '2022-10-04', '2022-10-07', '2022-10-09',
'2022-10-22', '2022-10-27', '2022-10-29', '2022-11-01', '2022-11-03', '2022-11-08',
'2022-11-23', '2022-11-26', '2023-02-01', '2023-02-11', '2023-02-14', '2023-02-19',
'2023-02-26', '2023-03-08', '2023-03-11', '2023-03-26', '2023-03-28', '2023-04-07',
'2023-04-10', '2023-04-12', '2023-04-15', '2023-04-25', '2023-05-10', '2023-05-15',
'2023-05-17', '2023-05-20', '2023-05-22', '2023-05-25', '2023-05-27', '2023-05-30',
'2023-06-01', '2023-06-04', '2023-06-09', '2023-06-14', '2023-06-16', '2023-06-21',
'2023-06-24', '2023-07-01', '2023-07-04', '2023-07-06', '2023-07-09', '2023-07-11',
'2023-07-19', '2023-07-21', '2023-07-24', '2023-07-29', '2023-07-31', '2023-08-03',
'2023-08-05', '2023-08-08', '2023-08-15', '2023-08-18', '2023-08-28', '2023-08-30',
'2023-09-04', '2023-09-09', '2023-09-14', '2023-09-17', '2023-09-19', '2023-09-22',
'2023-09-24', '2023-09-27', '2023-10-02', '2023-10-12', '2023-10-14', '2023-10-27',
'2023-11-13', '2023-11-28', '2023-12-13', '2024-02-19', '2024-02-21', '2024-02-24',
'2024-02-26', '2024-03-02', '2024-03-07', '2024-03-12', '2024-04-06', '2024-04-09',
'2024-04-14', '2024-04-19', '2024-04-21', '2024-04-24', '2024-04-26', '2024-05-01',
'2024-05-04', '2024-05-06', '2024-05-11', '2024-05-14', '2024-05-19', '2024-05-21',
'2024-06-03', '2024-06-10', '2024-06-23', '2024-07-03', '2024-07-13', '2024-07-15',
'2024-07-18', '2024-07-20', '2024-07-25', '2024-07-28', '2024-07-30', '2024-08-02',
'2024-08-07', '2024-08-09', '2024-08-12', '2024-08-14', '2024-08-24', '2024-08-27',
'2024-09-03', '2024-09-08', '2024-09-13', '2024-09-18', '2024-09-21', '2024-09-23',
'2024-09-26', '2024-09-28', '2024-10-03', '2024-10-06', '2024-10-08', '2024-10-18',
'2024-10-21', '2024-10-26', '2024-10-28', '2024-11-02', '2024-11-12', '2025-01-31',
'2025-03-17', '2025-03-27', '2025-04-01', '2025-04-06', '2025-04-11', '2025-04-16',
'2025-05-11', '2025-05-16', '2025-05-26', '2025-06-05', '2025-07-08', '2025-07-10',
'2025-08-07', '2025-08-14', '2025-09-01', '2025-09-13', '2025-09-15', '2025-09-16'
];

```

```
var s2_filter = filterImagesByDates(s2, dateList);
```

```
// Let's modify your date filter based on this
var s2_filter = s2_filter
  .filterBounds(torchLakeBbox)
  .filter(ee.Filter.eq('MGRS_TILE', '16TFQ'))
  //.filterDate('2018-12-13', '2018-12-25') // Starting from the first available date
  .linkCollection(csPlus, [QA_BAND])
  .map(addGBAIndices);

print('Number of images in filtered collection:', s2_filter.size());

// After your existing filters, add:
var firstImage = ee.Image(s2_filter.first());
var firstStats = computeStatsAndMasks(firstImage);
print('First image statistics:', firstStats.limit(1));

// Let's also print the specific pixel counts for the first feature
var firstFeature = ee.Feature(firstStats.first());
print('Pixel counts:', {
  'geometry_pixels': firstFeature.get('geometry_pixels'),
  'total_pixels': firstFeature.get('total_pixels'),
  'water_pixels': firstFeature.get('water_pixels'),
  'water_percentage': firstFeature.get('water_percentage')
});

// Process collection and compute statistics
var allStats = s2_filter.map(function(image) {
  return computeStatsAndMasks(image);
}).flatten();

// Export results
Export.table.toDrive({
  collection: allStats,
  description: 'Torch_Lake_Sentinel2_repro2024Nov25_on_2024Dec18',
  fileFormat: 'CSV'
});

// Print sample of results
print('Sample of statistics and mask counts by strata:', allStats.limit(5));

// Visualization parameters
var gbaViz = {
  bands: ['B3', 'B4', 'B2'],
  min: [300, 300, 300],
  max: [2000, 2000, 2000]
};
```

```

// Add layers to map for visualization
var count = s2_filter.size().getInfo();
print('Number of images after filtering:', s2_filter.size());
print(count)

var imageList = s2_filter.toList(count);

for (var i = 0; i < count; i++) {
  var image = ee.Image(imageList.get(i));
  var date = ee.Date(image.get('system:time_start')).format('yyyy-MM-dd').getInfo();
  Map.addLayer(image, gbaViz, 'Image ' + date, false);
}

// After the s2_filter definition, add:
// print('Number of images after filtering:', s2_filter.size());
print('First image date:', ee.Date(s2_filter.first().get('system:time_start')));
print('Sample image properties:', s2_filter.first());

Map.centerObject(torchLakeBbox, 11);
/*
// Example usage with your filtered collection
var allStats = s2_filter.map(function(image) {
  return computeStats(image);
}).flatten(); // Flatten because computeStats returns a feature collection for each image

// Export results
Export.table.toDrive({
  collection: allStats,
  description: 'torch_lake_stats_sept_2023',
  fileFormat: 'CSV'
});
*/

```{=latex}
\endgroup

```